Delft University of Technology

Faculty of Mechanical, Maritime and Materials engineering

Effects of $Li_4Ti_5O_{12}$ coating on the performance of $LiNi_{0.5}Mn_{1.5}O_4$ cathode in Li-ion batteries

Qiao Pan

Master of Science

Material Science and Engineering

28-08-2015

Effects of $Li_4Ti_5O_{12}$ coating on the performance of $LiNi_{0.5}Mn_{1.5}O_4$ cathode in Li-ion batteries

Abstract

Lithium ion batteries have attracted a lot of attentions due to the high power density and specific density that can potentially meet the requirements of new applications in the future. In recent years, one of the most promising cathode layer applied in lithium-ion batteries is called spinel $LiNi_{0.5}Mn_{1.5}O_4$ (LNMO), which has advantages of high electrochemical performance and low cost. However, the main disadvantage is the capacity fading during cycle test. Surface coating is recognized as an effective approach to reduce those negative influences. Theoretically, lithium titanate ($Li_4Ti_5O_{12}$, LTO), which has a similar lattice parameter with LNMO, could be a good choice.

In this project, spinel $LiNi_{0.5}Mn_{1.5}O_4$ layer was made on various substrate materials. Then, $Li_4Ti_5O_{12}$ is applied as an epitaxial coating on $LiNi_{0.5}Mn_{1.5}O_4$ layer. Both layers are made through electrostatic spray pyrolysis process. The samples with stainless steel substrate were made into coin cells, while the samples with aluminium substrate were made into Swagelok cells. XRD was used to identify the crystal structure. AFM and SEM were applied to observe the morphology of layers. In addition, the electrochemical properties information were obtained by charge-discharge cyclic test.

Key words: $LiNi_{0.5}Mn_{1.5}O_4$, $Li_4Ti_5O_{12}$ coating, electrostatic spray pyrolysis, spinel, electrochemical properties.

Content

List of Figures

List of Tables

Chapter 1 Introduction

Increasingly people realized that our society is facing a challenge of material scarcity and energy crisis. As estimated, traditional fossil fuels will run out in a few decades. For instance, oil as the most important conventional fossil fuel can only last for around 30 years[1]. Gradually, it will cause more and more serious problems as the year goes on if no strategies to be done. The reason can be attributed to two aspects. On the one hand, the increasing of the world population and the rapidly developing of economy lead our industrial society to a more resources dependent style, making the global consumption of materials increasing annually, while the resources in our planet are not infinite. On the other hand, the sound of protecting environment gets louder due to the high emission of green house gases during the process of manufacturing. Both aspects are driving not only the policy makers but also the researchers to find efficient methods to deal with those relevant problems.

Following this trend, it becomes important to think about renewable energy. As it is defined, renewable energy refers to the energy that comes from sources which are naturally replenished on a human timescale[2]. Some of these energies, such as wind, hydropower and solar energy, have been already used for a couple of years. However, these renewable energies have their own disadvantages. One problem related to renewable energy is that they usually fluctuate with day or season and can be influenced by weather and other factors, while the energy demand is always present. Another problem is that these kind of energies are heterogeneously distributed along the globe[3]. These problems indicate that it is necessary to find an convenient way to store and deliver these kind of energies. For these reasons, developing new batteries have been taken as a potential effective strategy by researchers and government officers from many counties, hence, to store electricity when it is available and deliver it when the demand is high.

1.1 Lithium-ion batteries

Over the past decades, many new electric products had been invented. New devices like electric vehicles (EV), hybrid electric vehicles (HEV), Mobile phones, MP3 players, digital cameras, laptop computers, etc., have greatly increased the happiness index of people' lives and continually promoted the development of technology to a new stage. Undoubtedly, the success of these inventions can not be achieved without the innovation of rechargeable batteries. While in the other aspect, along with the development of battery technologies, the world's population had been almost doubled in the recent half century. Consequently, there was an accelerating demand on these new products which in turn caused the dramatic increases of batteries. Figure 1.1 shows the exponential growth of lithium, nickel and cobalt batteries during the last 40 years[4].

Compared to other rechargeable batteries, such as nickel and cobalt batteries, lithium-ion batteries are seen as one of the most suitable candidates for power electronic portable devices. It was reported that the rechargeable batteries shared 70% of the global battery market size of $60 billion at 2010[5]. Figure 1.2 clearly shows the occupation rate of each battery in the market by a pie chart.

It can be found that Lithium-ion batteries occupied nearly 14% of the total market size, which equals approximately $9 billion. Although it still occupied a relatively small share of the global battery market at the beginning of this decennium, lithium-ion battery has already attracted a lot of attentions due to its special properties. It can be predicted that lithium-ion batteries will play a more important role in industry and academia in the future.

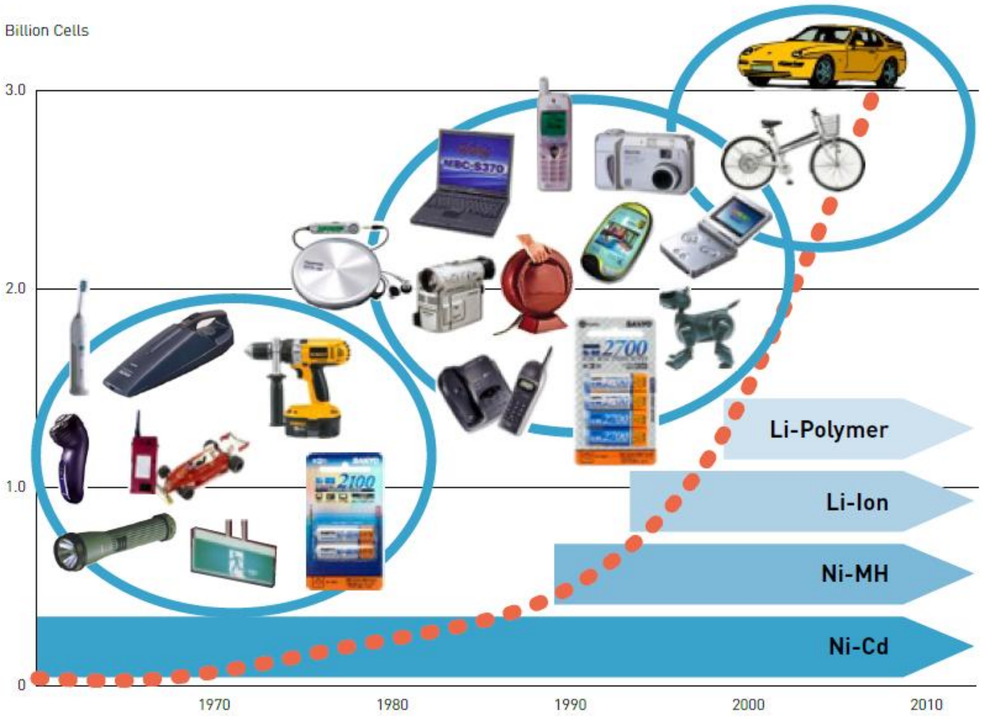

Figure 1. 1 Battery consumption in the nearest half century[4]

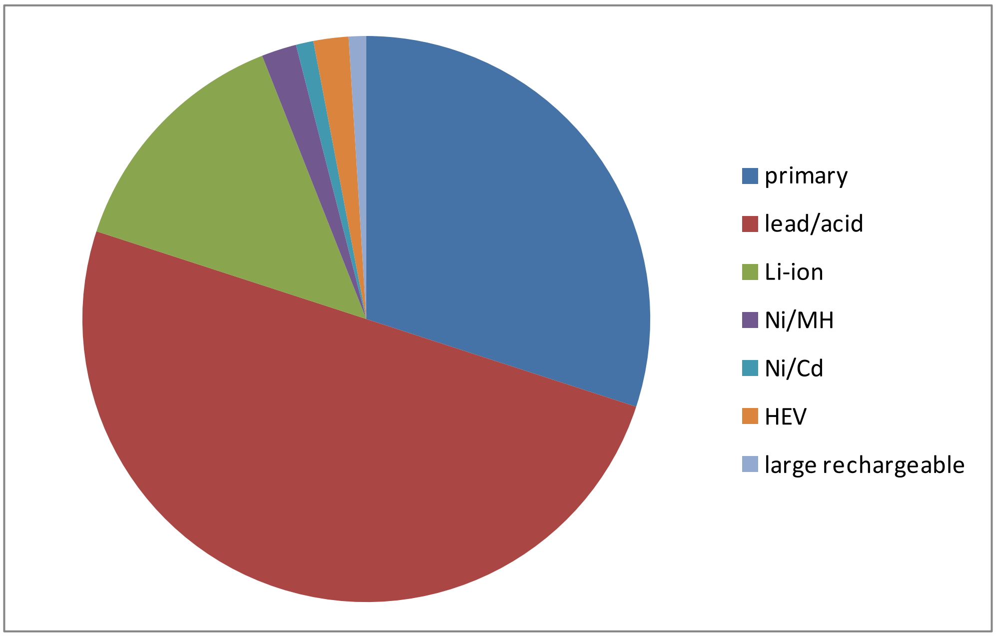

Figure 1. 2 market occupation of different batteries[4]

1.1.1 A brief history of lithium-ion batteries

Batteries as one of the most common energy storage devices have a history of more than 200 years. Starting from 19th century, both primary and secondary (rechargeable) batteries have experienced great development since the first battery was invented by Alessandro Volta at 1800[6]. However, it was improved slowly for more than a century because the conventional batteries met the requirements of technology at that period of time. This situation changed dramatically in the 1960s due to the explosive innovations in military and electronics. Soon after that, it was realized that it would be the time for conventional batteries to step off the stage of history because they could no longer meet the new requirements of the fast-developing technologies[7].

Lithium-ion battery as one type of the secondary batteries was first proposed by M.S. Whittingham in the 1970s[8-9]. Compared to conventional batteries, i.e., alkaline–manganese, nickel–cadmium, or lead–acid, this kind of battery has a higher energy density and specific density that can meet the requests of new applications at that period of time. Figure 1.3 shows the difference of energy density and specific density between lithium battery and some typical other conventional batteries. Table 1.1 gives more details about the differences in energy density and cyclic lifetime of some typical batteries[10]. In order to produce this rechargeable lithium-ion battery, a compound that can allow lithium ions reversibly passing through their open structure was needed. Based on this idea, it was soon found that transition metals can meet the requirements by changing a charge from IV to III in the valence state. Then, at the beginning of 1980s, a couple of early commercial rechargeable lithium-ion batteries were invented by some companies in North America[11].

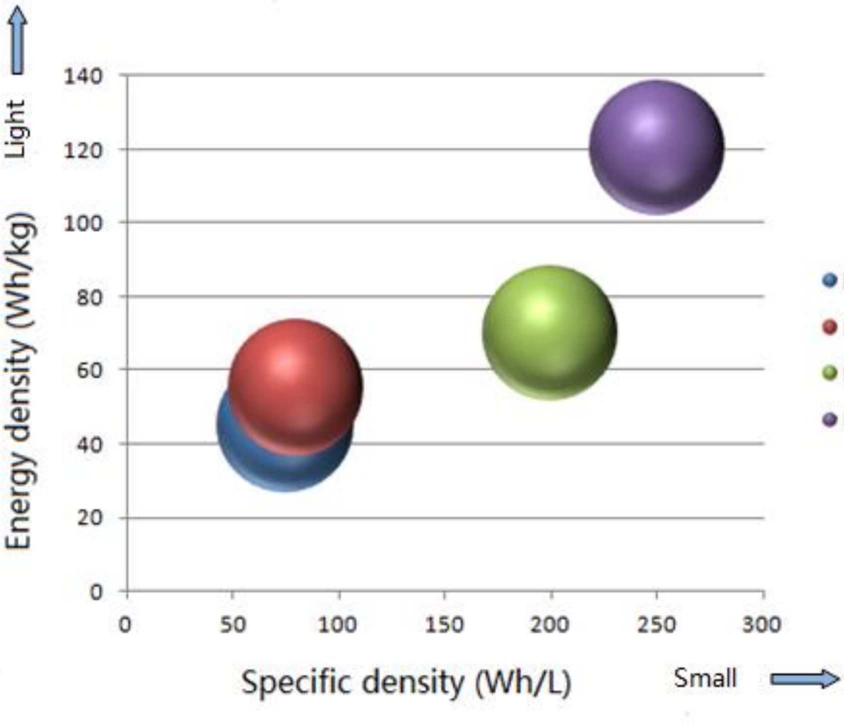

Figure 1. 3 Electrochemical properties of several batteries

Table 1. 1 Energy density and lifetime of several batteries[10]

Battery type	Energy density (Wh/kg)	Lifetime (cycles)
Nickel-cadmium	45-80	1500
Ni-MH	60-120	300-500
Lead-acid	30-50	200-300
Lithium-ion	110-160	300-500
Lithium-ion-polymer	100-130	300-500
Reusable alkaline	80	50

However, these lithium batteries also have some disadvantages. A common problem related to safety issues due to the active anode and a so called solid electrolyte interface(SEI) formed during the charge-discharge process[12]. These disadvantages act as a driving force for researchers to improve the properties of batteries. Then, some years later when an efficient lithium polymer battery was invented, a new system called lithium rocking chair battery was introduced to the public[13].

Basically, this new concept consists of an anode that can accept lithium ions and a cathode that acts as a lithium ion source. It was in 1991 that the first application was made by the Japanese company Sony[14]. Besides graphite was used as anode, the cathode material was replaced by lithium cobalt oxide($LiCoO_2$), which still can be found in many commercial products today. A typical structure of the $LiCoO_2$ battery is shown in Figure 1.4[15].

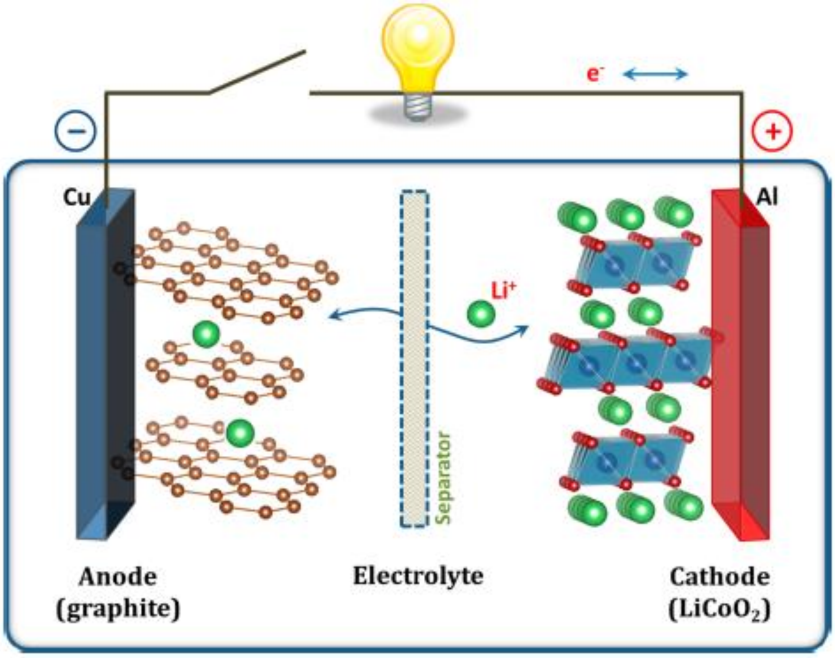

Figure 1. 4 A typical structure of $LiCoO_2$ battery[15]

1.1.2 New challenges

As it was mentioned at the beginning of this chapter, material scarcity and environment deterioration are attracting more and more attentions of our society, making new requirements to the next generation of products. Consequently, energy saving and cost reducing becomes the hot topics in many fields, resulting in a revolution of technologies. Under such circumstances, a number of new applications, such as microelectronic devices, hybrid vehicles and electric vehicles as well as renewable energy plants, were invented. Meanwhile, plenty of new chances for business competitors were created. However, new chances always accompany with new challenges. Power sources with high energy density are needed for electronic devices and environmental friendly vehicles, and so do the energy storage systems for wind and solar energy. Fortunately, lithium-ion batteries have the potential to be the ideal choice for these purposes due to the good performance on energy density[16]. But on the other side, it should be realized that the limitations, which can bring negative influences on the development of lithium-ion batteries, also exist at present. For instance, liquid electrolyte has safety problems, cobalt is expensive, energy density is not high enough, etc,.. Therefore, increase safety, reduce cost and further enhance energy density are in turn to be the main challenges that need to be taken into account in the future[17-19].

Recently, a number of researches have proposed new ideas in order to minimize these negative influences. Using ionic liquids to replace $LiPF_6$ electrolyte which was widely used at present could be an efficient method to solve safety problems. Similarly, another replacement which is called solid electrolyte was studied by some research groups. Meanwhile, some other scientists focus on reducing the cost of batteries. Instead of using rare earth element, new cathode materials, such as $LiMn_2O_4$ and $LiFePO_4$, were developed in recent years. Compared to the conventional lithium batteries, super-batteries, e.g. lithium-sulfur and lithium-air batteries, with even higher theoretical energy density had been already taken into experimental stage.

Michel Armand[20] explained that ionic liquids have possibilities to solve the safety problem since they are non-flammable. Using Ionic liquid to replace liquid electrolyte can reduce the risk of thermal runaway. However, some new phenomenon were observed and need to be studied. For instance, the formation of passive layer on electrode and the structure of the interfaces between electrode and electrolyte.

Another method to enhance the safety standard of lithium-ion battery is to use polymer electrolyte. Normally, the limitation of polymer electrolyte is the low ionic conductivity at room temperature. It was 11 years ago that Joon-Ho Shin[21] prepared a "$PYR_{13}TFSI$ + $P(EO)_{20}LiTFSI$" polymer electrolyte film with the ionic conductivity reached 10^{-4} S/cm at room temperature. In the research, Shin also studied the influence of different molar fraction of PYR_{13}^+/Li^+.

Since the first lithium rocking chair battery was invented in 1991, it dominated the market for more than 15 years and still can be found in many commercial products today. Basically, the cathode material of this kind of battery was replaced by lithium cobalt oxide($LiCoO_2$), which increased the price. In order to reduce the cost, D.Singh[22] prepared a spinel-structured $LiMn_2O_4$ film on various substrate materials by using an ultraviolet assisted pulsed laser deposition process. According to testing results, it also gave an enhancement in electrochemical properties, such as larger capacity, longer cycle life and higher discharge rate capacity. However, this new cathode material still has the problem of forming solid electrolyte interface during cycle process. Thus, further improvements are needed.

A.K.Padhi's research[23] on Phosphor olivines indicated that $LiFePO_4/FePO_4$ can be a good candidate as the cathode of lithium rechargeable batteries for low power applications. It also pointed out that capacity fade which might be caused by the movement of $LiFePO_4/FePO_4$ interface is one of the limitations.

Although lithium batteries have a high theoretical energy density, it still can not submit the requirement of some high-power-demanded devices, such as electric vehicles. In recent years, Yan Zhao[24] introduced the new development of the combination between lithium/sulfur battery and polymer electrolyte, which gives an possibility to prepare super batteries with even higher energy density compared to conventional lithium batteries. In addition, Yan also mentioned the main problem is the poor cyclic ability which is mainly due to poly-sulfides dissolving into the electrolyte.

All these researches demonstrate the initial efforts that had been done in order to enhance the properties of lithium-ion batteries. However, those improvements are in an early stage and still can not meet the requirements of new generation products. Therefore, more efforts need to be made. Further researches focused on new materials or their derivatives could be a way to achieve the goals.

1.2 $LiNi_{0.5}Mn_{1.5}O_4$ as cathode material

As it was mentioned above, a number of new compounds were applied into lithium battery in recent years in order to improve the properties. Among those compounds, $LiNi_{0.5}Mn_{1.5}O_4$(LNMO) is one of the most promising materials used as cathode due to its high voltage, high-energy density, high-rate capability and low cost.

1.2.1 Crystal structure of $LiNi_{0.5}Mn_{1.5}O_4$ and properties

$LiNi_{0.5}Mn_{1.5}O_4$ can be taken as a derivative of $LiMn_2O_4$ with 1/4 Mn ions substrate by Ni ions. A LNMO has two typical crystal structures, which are called face-centered spinel (Fd3m) and primitive simple cubic crystal ($P4_332$), respectively. For LNMO with the spinel structure, all the Mn ions and Ni ions are randomly distributed at octahedral sites of the face-centered cubic, forming a disordered structure. While in the primitive simple cubic structure, Mn ions and Ni ions can only occupy 12d sites and 4a sites, respectively, forming an ordered structure. A schematic drawing of the spinel LNMO crystal structure can be seen in Figure 1.5. Previous studies indicate that spinel disordered structured LNMO shows a better performance on cycling and rate capability than that of ordered structure due to a small amount of Mn^{3+} exist[25-26].

Different from that in layered $LiCoO_2$ structure and olivine $LiFeO_4$ structure, the diffusion path of lithium ion in spinel structure is a three-dimensional network (Figure 1.6). In order to diffuse from one tetrahedral site to another though interstitials in the crystal structure, lithium ions need to overcome the activation barrier of migration which can be largely influenced by the electrostatic repulsion from the nearest atoms[27]. While a small amount of Mn^{3+} in spinel structure will cause expansion of lattice due to its larger ionic radius compared to that of Mn^{4+}. Lithium ions can move more freely in a expanded lattice. Thus, the diffusion rate of lithium ions increase[28].

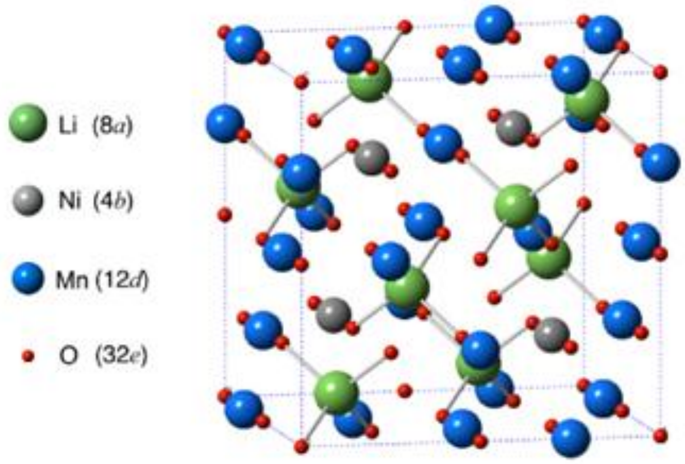

Figure 1. 5 Crystal structure of spinel LNMO [25]

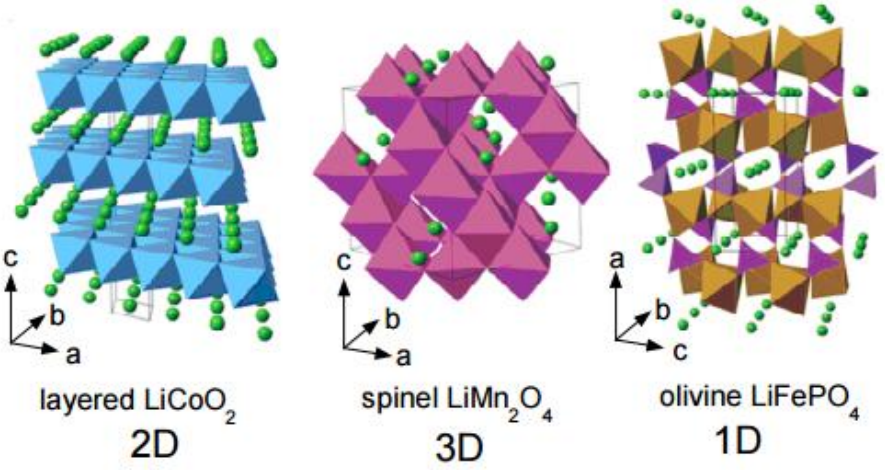

Figure 1. 6 Dimensionality of the lithium ions transport[27]

Not only do the presence of nickel and manganese ions allow a contribution in forming the spinel structure, but also they play an important role in giving LNMO excellent electrochemical properties. Spinel LNMO has a theoretical capacity of 147mAhg^{-1} and high discharge voltage plateaus at around -4.1V and -4.7V, which gives a 20% higher energy density relative to $LiCoO_2$[29]. Plenty of previous researches pointed out that the presence of high voltage plateaus are related to the redox behavior of nickel and manganese ions[30-32].

1.2.2 Synthesis of LNMO

Attracted by the high performances of LNMO, researchers have developed a number of methods for preparing face-centered spinel LNMO thin layer. Among those methods, the most frequently applied are solid-state reaction and wet chemical method[33]. Solid-state reaction is a simple method that usually contains the process of heating precursor mixtures to high temperatures in order to get the reaction products. Wet chemical method is a common name for a group of methods used for making products from solutions, including sol-gel method, spray drying and post annealing, polymer-assisted synthesis, etc,. Usually, wet chemical methods require lower temperature and less time for making final products compared to that of solid-state reaction. In addition, it should be clear that the parameters applied in these synthesis methods can strongly influence the structure and properties of LNMO. Researches were investigated that a lattice structure transformation will happen under a certain annealing temperature and duration[34]. Also, some other researches found that the detrimental impurities formed when synthesized at a high temperature[35].

In recent years, several new wet chemical methods for synthesizing nano-sized LNMO spinels have been developed. For instance electrospray deposition pyrolysis[36-37], ultrasonic spray pyrolysis[38], pulsed laser deposition[39] and composite carbonate process[40]. In these methods, Li, Ni and Mn salts are usually dissolved into a solvent and mixed homogenously at atomic scale. By further drying processes, nano-sized LNMO particles can be formed at low temperatures. Due to nano-size effects, several advantages can be achieved. The transport path length for lithium ions and electrons can be shorter. Also, the contact area between electrode and electrolyte can get larger, resulting in higher cycling rates. However, according to the mechanism of thermodynamics and kinetics, these LNMO particles could grow to larger sizes and then lose nano-size advantages if the temperature goes too high or the annealing process lasts too long[41].

1.2.3 Disadvantages and improvements

As it mentioned above, spinel LNMO has been recognized as an excellent candidate for making cathode material in Li-ion batteries due to its remarkable properties. However, the main disadvantage of this cathode layer is the fast capacity fading during the charge-discharge cyclic test[42]. Some researches indicated that such capacity degradation could be attributed to Mn and Ni dissolves into liquid electrolyte, causing decomposition of electrolyte on electrode surface[43-44]. In order to overcome this problem, several approaches have been selected. One of the ideas is to improve the interface between LNMO and liquid electrolyte[45]. Others are based on the idea of replacing one of the elements in this cathode system, including substitution Mn or Ni by Mg, Co, Cr, Zn, etc., to ease the phenomenon of metal losing, develop new electrolytes to replace HF-contained $LiPF_6$-based electrolytes, partial replace the O in LNMO by F to increase the stability of the host structure[46-49]. Among these approaches, surface coating is recognized as an effective approach to avoid direct contacting between LNMO and electrolyte or replace the liquid electrolyte as a solid electrolyte. Several coating materials, such as ZnO, Al_2O_3, SiO_2, etc., have been used as the interface stabilizers and proven to be effective in reducing the electrolyte decomposition[50-52]. On the other hand, these coating materials were taken as the inappropriate choices for lithium-ion battery. First, it is easy to peel-off from the electrode surface during charge-discharge process attributed to the weak bonding between coating and substrate material. Second, large structure mismatch exists between coating and substrate material, leading to stacking faults which can block the diffusion path for lithium ions. Last, the ion conductivity of these coating materials are relatively low[53]. Therefore, new coating materials that can match the requirements for lithium-ion batteries, especially for LNMO cathode layer, need to be developed.

1.3 Spinel $Li_4Ti_5O_{12}$

Similar to the crystal structure of spinel LNMO, lithium ions and oxygen ions in the spinel $Li_4Ti_5O_{12}$(LTO) are occupied the 8a and 32e positions, respectively. All the titanium ions are occupied the 16d positions[54]. When lithium ions insert into spinel LTO structure, an insertion reaction $\mathrm{Li_4Ti_5O_{12} + 3Li^+ + 3e^- \rightarrow Li_7Ti_5O_{12}}$ takes place. Lithium ions will be stored in the octahedral sites in the new forming rock salt-type $Li_7Ti_5O_{12}$[55]. Figure 1.7 shows the structure difference in these two crystals.

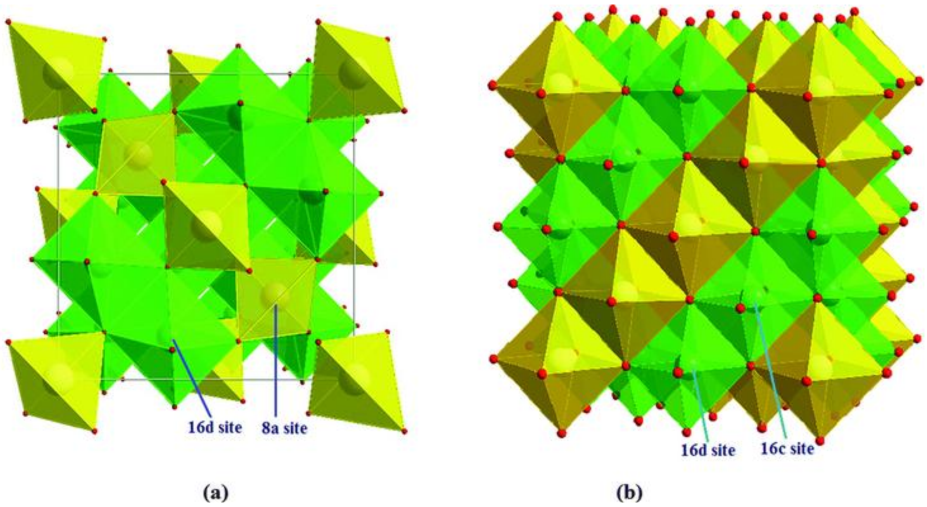

Figure 1. 7 crystal structure of LTO before (a) and after (b) the insertion of lithium ions [55]

1.3.1 $Li_4Ti_5O_{12}$ as an anode material

It is common to find that spinel lithium titanate ($Li_4Ti_5O_{12}$, LTO) was used as an alternative anode material in lithium-ion batteries in many research works. LTO with a spinel structure allows lithium ions to insert and extract, giving it a possibility to become an anode part in lithium-ion batteries. According to the results of many previous electrochemical tests, LTO can provide a stable voltage of 1.55V against a lithium electrode. It usually needs to be coupled with a cathode, such as $LiFePO_4$ with a voltage of 4V acts as a lithium ion source, to assemble to be a battery cell[56].

Coupling with LNMO cathode material, LNMO/LTO was considered as a new lithium-ion battery system. This battery system has a output voltage of more than 3V since the operating voltage of LNMO cathode can reach 4.7V and that of LTO is around 1.55V, respectively[57]. The spinel LTO anode had been considered as a “zero-strain” insertion material for accepting lithium ions due to its reversibility and stability in the cycling process. Since the structure of LTO has a excellent stability in the liquid electrolyte, it was considered to be safer than graphite, which was used as anode in the old battery systems[58].

1.3.2 Li$_4$Ti$_5$O$_{12}$ as a coating material

Theoretically, spinel LTO also has the potential to be the coating material of LNMO cathode. The lattice parameter of LTO is close to that of LNMO, which makes it possible to form an epitaxial LTO coating on LNMO. At a same temperature of 800℃, the lattice parameter of spinel LTO is 8.248Å, while that of LNMO is 8.176Å, approximately[59]. The lattice mismatch is less than 1% which means almost no stacking faults will be formed. Thus, there will be little barrier on lithium ion diffusion. Further, the spinel structure of LTO create a three-dimensional network path which allows lithium ions pass through. Hence, it is reasonable to expect that the thin and homogenous spinel LTO coating layer of LNMO cathode can be a solid electrolyte applied in lithium-ion batteries, provided LTO will not electrochemically insert lithium ions. Figure 1.8 and 1.9 show the idea of depositing a LTO coating on LNMO cathode layer.

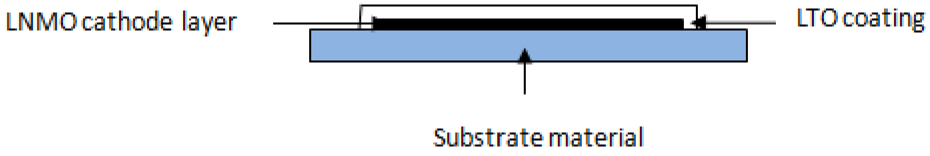

Figure 1. 8 The structure of the LTO-coated LNMO cathode layer

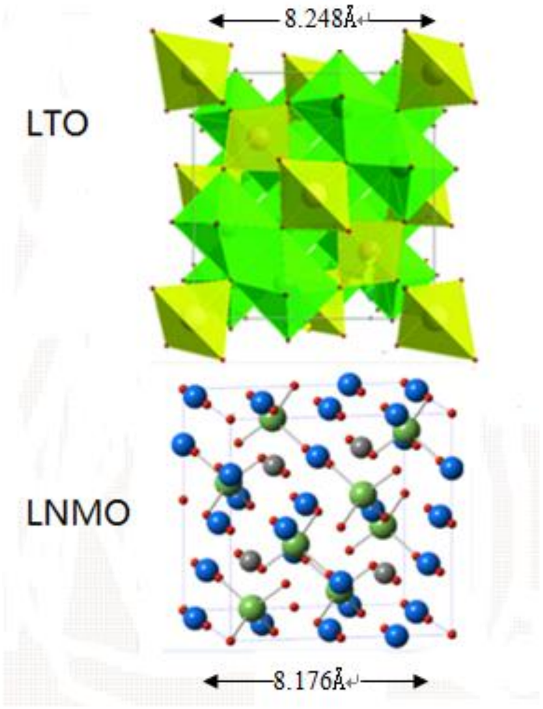

Figure 1. 9 The lattice structure of LTO covered LNMO

Some relative researches have been already done to the $Li_4Ti_5O_{12}$ coating layers and its derivatives. It was 20 years ago that Tsutomu Ohzuku's research[60] indicated that $Li(Li_{1/3}Ti_{5/3})O_4$ can be used as a zero-strain coating material applied in lithium-ion batteries. Some years later, Tingfeng Yi[61] studied the crystal structure of $Li_4Ti_5O_{12}$-coated $LiMn_{1.4}Cr_{0.2}Ni_{0.4}O_4$ layer by X-ray diffraction. He also indicated that the weight percentage of these cathode layer would influence the electrochemical property of batteries. Soon after that, Na Li[62] mentioned the main disadvantage of LTO is the low electronic conductivity and moderate Li-ions diffusion coefficient. Recently, Jili Li[63] studied the interface between the spinel epitaxial $Li_4Ti_5O_{12}$ coating layer and $LiMn_2O_4$ cathode layer by high resolution transmission electron microscopy (HR-TEM) and high angle annular dark field scanning transmission electron microscopy (HAADF-STEM) with atomic resolution images. It was proven that $Li_4Ti_5O_{12}$-coated cathode exhibited better cyclability, thermal and rate capability for lithium-ion batteries compared to that of un-coated $LiMn_2O_4$ cathode. At the same year, Haifu Deng[64] prepared a Li_2TiO_3-coated $LiNi_{0.5}Mn_{1.5}O_4$ cathode and proved that the capacity was still high after 50 discharge/charge cycles. All these researches indicated that $Li_4Ti_5O_{12}$ and its derivatives have the potential to be the coating materials of LNMO cathode layer and at the same time act as a solid lithium ion conducting electrolyte.

1.3.3 Synthesis methods

Several synthesis methods of LTO coating layer were also mentioned in literatures. Hydrolysis[65], solid-state reaction[66], sol-gel[67], electrochemical deposition[68], and chemical spray pyrolysis[69] are the most frequently mentioned methods used by researches. These methods can lead to different microstructures of coating layers, which in turn cause differences in properties.

1.4 Electrostatic spray deposition applied in lithium-ion batteries

Electrostatic spray deposition(ESD), which is also called electrospray deposition or electrohydrodynamic atomization, is a process of depositing thin film layers onto various substrates[70]. The charged liquid precursor will be sprayed out from a capillary nozzle into a build-in electric field where it will be dispersed into tiny droplets. These dispersed droplets will eventually reach the substrate and then form a coating layer after the liquid evaporates. This technique can be both used in industry and scientific research. In recent years, it has been developed and applied into nano-technologies. Coupled with other assisted methods, ESD can be designed to make functional layers used in different advanced products. For instance, lithium batteries, solar cells, functional ceramics, etc.[71].

As it is mentioned in section 1.2.2 and 1.3.3, ESD is a feasible method for making a cathode layer as well as its coating layer in lithium-ion batteries. Usually, it is coupled with a heating source which is connected to the substrate. Since the liquid precursor was evaporated soon after it reached the substrate, a solid thin film can be deposited. It can be found that this process is also called electrostatic spray pyrolysis(ESP) in number of literatures[72-73].

The equipment of electrostatic spray pyrolysis consists of two systems, including the spray system and the control system. Figure 1.10 shows a schematic drawing of the ESP equipment[74]. The former system is designed for spraying the liquid precursor onto the surface of the target automatically, while the latter system is used for controlling the voltage and temperature. The precursor is filled into a syringe fixed at the pump. The syringe is connected to a metal capillary nozzle by a rubber hose. A electric field is created between the nozzle and the substrate holder by applying a high voltage. A number of parameters are chosen and applied manually. The thickness and the surface morphology of the deposited layer can be greatly influenced by those parameters. For instance, the distance between the nozzle and the substrate holder, the temperature of the holder, the voltage, the spray volume and the flow rate.

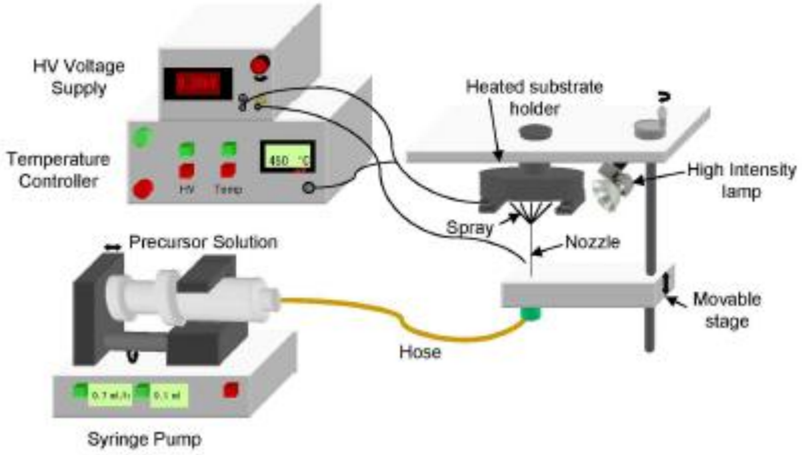

Figure 1. 10 A schematic drawing of the ESP setup[74]

1.5 Research question and the structure of this thesis

The research question of this project is to study the possibility of using LTO as a potential solid lithium ion conducting electrolyte. As a direct derivative, LTO coatings on cathode materials, such as LNMO, may protect these cathode materials, so as to prevent solid electrolyte interphase growth and dissolution of manganese in a liquid electrolyte. In order to do so, a

In this project, all the samples were made by electrostatic spray pyrolysis process. Spinel $LiNi_{0.5}Mn_{1.5}O_4$ layers were sprayed onto different substrate materials as the cathode layer. Then, spinel $Li_4Ti_5O_{12}$ was applied as an epitaxial coating layer onto $LiNi_{0.5}Mn_{1.5}O_4$ layer. The samples with stainless steel substrate were made into coin cells in a glove box. XRD tests were used to identify the spinel structure. AFM and SEM were applied to observe the morphology of layers. In addition, the electrochemical properties results were obtained from the charge-discharge cyclic test.

This thesis consists of four chapters. Including this introduction, a brief outline of the other three chapters are shown below.

Chapter 2 is a detailed introduction of experimental setups and testing methods. The materials and reagents, the initial parameters and the advanced testing instruments are all introduced systematically. Additionally, all the samples that made through ESP are illustrated.

Chapter 3 is a presentation of quantitative and qualitative data that were obtained from the tests. Based on these data, the results were analyzed and thus discussed.

Chapter 4 is a conclusion of this thesis based on the discussions in chapter 3.

Chapter 2 Experiments

In this chapter, the experimental details will be introduced. At first, all the reagents and materials that were used in the experimental stage will be shown. Further, the sample preparation process will be introduced in details, including the substrate cleaning methods, LNMO layer spray process and LTO coating spray process. Last, the information of all the testing methods used in this project will be given.

2.1 Reagents and materials

In this project, the used reagents and materials can be divided into 3 parts, including reagents and materials used in the precursor preparation, in the substrate material cleaning process and in the cell assembly. The details of all the reagents and materials used in this project can be read in Table 2.1.

Table 2. 1 Information of the used reagents and materials

processes	Reagents and materials	company
Precursor preparation	$LiNO_3$	ReagentPlus
	$Ni(NO_3)_2 \bullet 6H_2O$	Alfa Aesar GmbH
	$Mn(NO_3)_2 \bullet 4H_2O$	Alfa Aesar GmbH
	$C_{12}H_{28}O_4Ti$	Aldrich
	2-Propanol	Sigma-Aldrich
Substrate material and the cleaning process	Silicon wafer	
	Stainless steel coin cell cap	
	Acetone	VWR
	Methanol	J.T.Baker
	Ethanol	VWR
Cell assembly	Polyethylene	Solupor
	$LiPF_6$	Aldrich
	Metallic Lithium	

2.2 Sample preparation

Before starting the electrostatic spray pyrolysis experiment, the precursor solutions need to be prepared with the appropriate precursor ratios, so as to respect the final LNMO stoichiometry. In addition, the surfaces of the substrate materials need to be cleaned following the procedures. After finishing all these steps, LNMO layer and LTO coating can be deposited onto the substrate materials through ESP.

2.2.1 Precursor preparation

The precursor used for making LNMO layer was prepared from lithium nitrate, $LiNO_3$

(ReagentPlus), nickel nitrate hexahydrate, $Ni(NO_3)_2 \cdot 6H_2O$ (Alfa Aesar GmbH) and manganese nitrate hydrate, $Mn(NO_3)_2 \cdot 4H_2O$ (Alfa Aesar GmbH). These salts were weighted, and then dissolved in 2-propanol following the spinel stoichiometry. The Li:Ni:Mn molar ratio in the solution is 2:1:3, respectively. In order to form a thin LNMO layer, the concentration of the prepared solution was controlled to be 0.05mol/L based on 0.34g of $LiNO_3$, 0.707g of $Ni(NO_3)_2 \cdot 6H_2O$ and 1.63g of $Mn(NO_3)_2 \cdot 4H_2O$ dissolved into 100ml of 2-propanol. No polymeric binder or conductive additive was added to the precursor solution.

Similarly, the precursor used for making LTO coating layer was prepared from $LiNO_3$ (ReagentPlus) and titanium (IV) isopropoxide 97% ($C_{12}H_{28}O_4Ti$) by dissolving into 2-propanol following the spinel stoichiometry. The Li:Ti molar ratio in the solution is 4:5, respectively. Note that the LTO coating should be fully cover the LNMO layer. In order to achieve this goal, the concentration of the prepared solution was controlled to be 0.1mol/L based on g of $LiNO_3$ and g of $C_{12}H_{28}O_4Ti$ dissolved into 100ml of 2-propanol. The prepared solutions are shown in Figure 2.1.

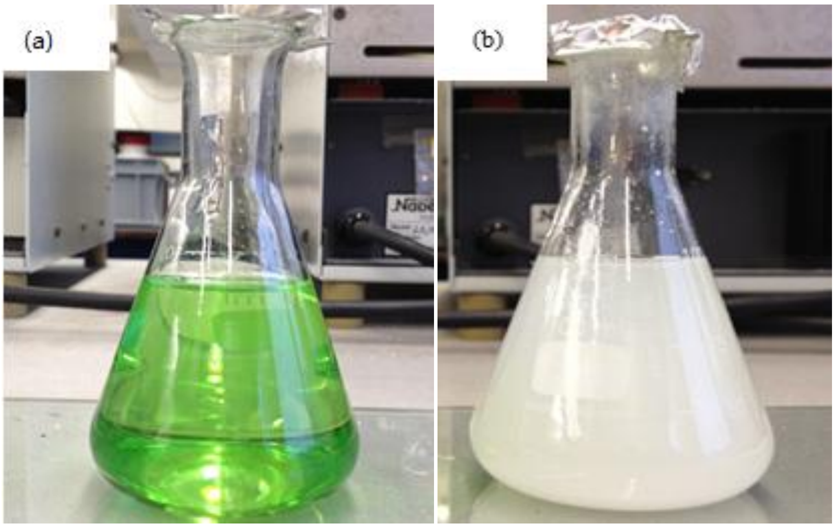

Figure 2. 1 Precursor solutions of LNMO (a) and LTO (b)

2.2.2 Substrate cleaning method

In order to deposit thin and homogenous cathode layers on the substrate material, the surface of the substrate material should be flat. However, it can not be avoided that some inorganic and organic residues, such as dust and chemical particles, will adhere onto the surface when storing or moving those materials. These unwanted contaminates can decrease the surface condition and that in turn will influence the properties of the deposited layers. Moreover, these particle contaminates are not easy to be removed due to the strong electrostatic force between the particles and substrate. Therefore, it is necessary to clean the substrate material by following an efficient cleaning procedures.

In this project, silicon wafers and stainless steel coin cell caps were cleaned by following a two-solvent cleaning procedure introduced by the University of California Irvine[75]. The cleaning steps can be found in Table 2.2.

Table 2. 2 Cleaning procedure[75]

Steps	Process	Effect
1	Place the substrate into acetone bath for 10 minutes	Dissolve the organic particles
2	Place the substrate into methanol for 5 minutes	Dissolve the acetone residues
3	Place the substrate into ethanol for 5 minutes	Further cleaning
4	Dry the substrate by air	Remove ethanol residues

2.2.3 Gold sputtering of silicon wafer

Silicon wafer is frequently used as the substrate material for deposition of various materials applied in microelectronic devices manufacture. The wafer was grown from crystals with regular crystal structure. Usually, the wafer surface is aligned in one of the specific crystal orientations. Thus, the cleaned surface of silicon wafer is flat which meets the requirement for depositing a uniform layer. However, when it is applied as cathode substrate, the electrochemical properties of the assembled battery could be limited due to the low electron conductivity as a result of the indirect bandgap of silicon (1.12eV at 300K)[76].

Gold sputtering is an efficient method to overcome this disadvantage. By forming a thin gold coating, the electron conductivity of the sample can be significantly improved. The sputtering process was done by using an auto fine coater (JEOL JFC-1300). The silicon wafer was placed in the chamber fulfilled with Ar gas. By applying a high voltage for 2-3mins, a homogenous gold coating was formed on the wafer surface. The samples were shown in Figure 2.2.

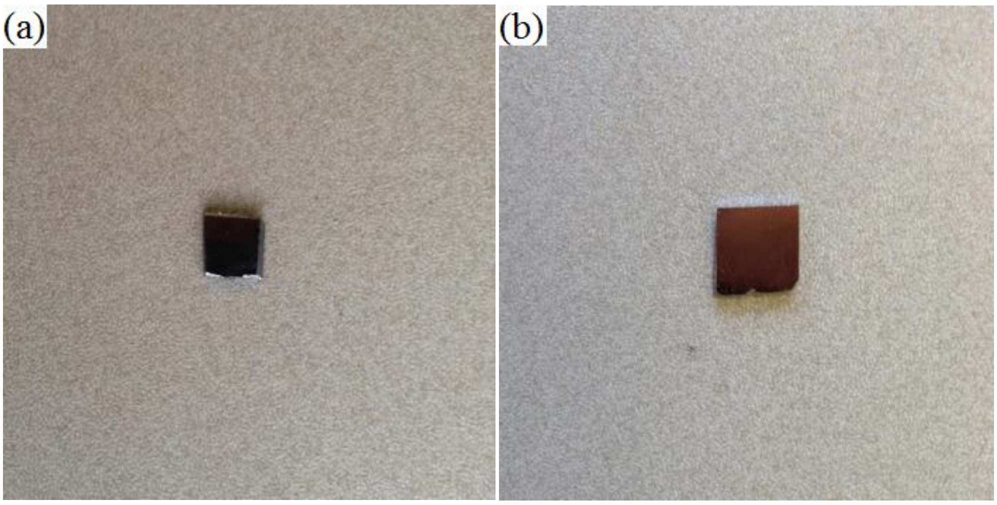

Figure 2. 2 Silicon wafer before (a) and after (b) gold-coated

2.2.4 LNMO cathode layer

As it was described in section 1.4, electrostatic spray pyrolysis(ESP) was used to form LNMO cathode layer on various substrates. The prepared precursor solution was fed to the electrified nozzle automatically from a controlled pump to the heated substrate holder where the chemical reactions took place at the certain temperatures. In this experiment, the reaction that took place during pyrolysis of the used precursors is simplified as follows:

$$\mathrm{Li(NO_3)} + \mathrm{Mn(NO_3)_2 \cdot 4H_2O} + \mathrm{Ni(NO_3)_2 \cdot 6H_2O} + \mathrm{O_2} \xrightarrow{450℃} \mathrm{LiNi_{0.5}Mn_{1.5}O_4} + \mathrm{H_2O} \uparrow + \mathrm{CO} \uparrow + \mathrm{NO_2} \uparrow + \cdots + \mathrm{CO_2} \uparrow$$

A number of parameters were chosen in order to form a stable electrospray in the so called cone-jet mode so as to form a homogenous thin layer.The temperature at which the film deposition was performed was chosen at 450℃. The optimized voltage can vary from 6.5 to 9.5kV as a function of the liquid precursor used. A dispensing tip (EFD R Nordson) with inner diameter of 0.1mm was applied during all the electrospray experiments. The distance between nozzle and substrate was set to be 2.5cm. The flow rate and the spray volume applied were 0.3ml/h and 0.01ml, respectively. In addition, an annealing process was applied after the spray process in order to form dense layers. All the deposited substrates were annealed at 450℃ in air for one hour. All the parameters chosen in these experiments were following the previous research results in our research group[77]. Table 2.3 shows the values of all the parameters that were used in these experiments. By following these parameters, a couple of samples with LNMO cathode layer were made. Figure 2.3 shows the pictures of the samples with different substrates made through ESP by following the parameters mentioned above.

Table 2. 3 Electrospray parameters for making LNMO layer

Parameter	Value
Precursor concentration	0.05mol/L
Temperature	450℃
Voltage	6.5-9.5kV
Inner diameter of nozzle	0.1mm
Distance between nozzle to substrate	2.5cm
Flow rate	0.3ml/h
Spray volume	0.01ml
Spray time	2mins
Annealing temperature	450℃
Annealing time	1h

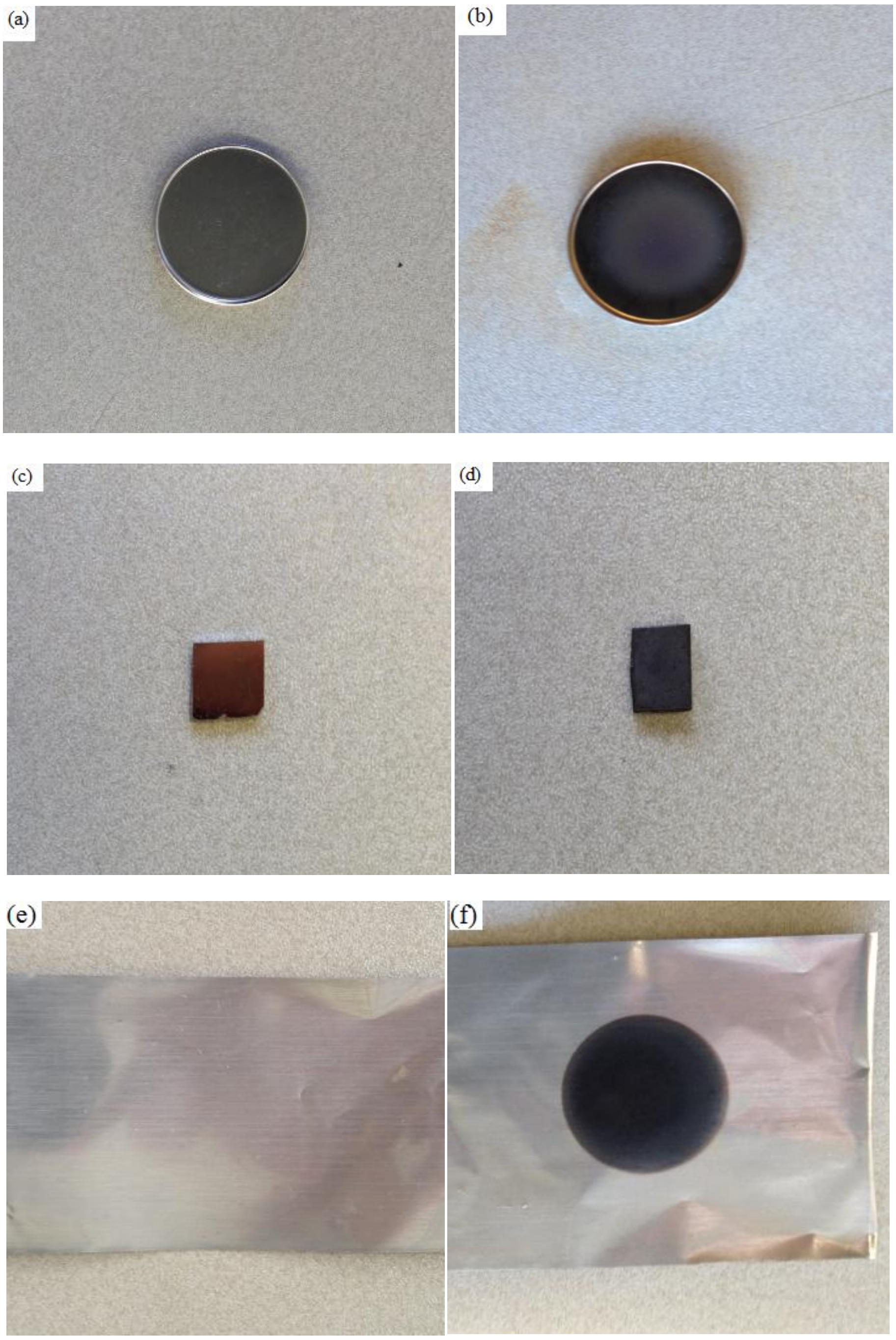

Figure 2. 3 Samples with made by ESP: CR2320 coin cell cap before (a) and after (b) deposited by LNMO layer; gold coated silicon wafer before (c) and after (d) deposited by LNMO layer; aluminium foil before (e) and after (f) deposited by LNMO layer.

2.2.5 LTO coating layer

LTO coatings were also made through the ESP process. Similar to the process of making LNMO cathode layer, the prepared precursor solution was filled into a syringe placed on the syringe pump. Controlled by the parameters, such as flow rate and spray volume, it was automatically sprayed onto the heated substrate holder where the sample with a LNMO cathode layer fixed. The chemical reaction took place during pyrolysis of the used precursor solution was simplified as follows:

$$LiNO_3 + C_{12}H_{28}O_4Ti + O_2 \xrightarrow{400-450℃} Li_4Ti_5O_{12} + H_2O\uparrow + NO_2\uparrow + CO\uparrow + \cdots + CO_2\uparrow$$

As the precursor used for LTO coating deposition was different from that of LNMO layer, many chemical and physical properties were also different. For instance, viscosity, surface tension, conductivity, absolute permittivity, etc.. This led to a further difference in the parameters applied in ESP systems. In order to deposit a homogenous thin coating on LNMO layer, a group of effective parameters were found during the experiments. It should be noticed that the optimized temperature of the substrate was found to be 415℃. A lower temperature could lead to porous morphology as the liquid can not evaporate immediately after it reached the host material. While a higher temperature always made it very easy to lose the cone-jet mode because solid particles were gathered at the nozzle tip due to the fast evaporation of the 2-propanol solvent. This phenomenon is illustrated in Figure 2.4.

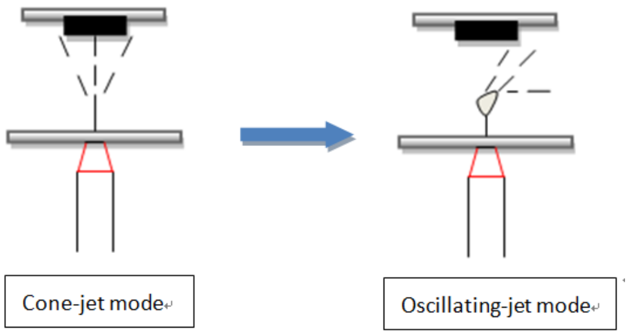

Figure 2. 4 Spray mode changes during LTO coating spraying process

Other parameters, including concentration, voltage, flow rate and annealing temperature, were all different from that applied to deposit LNMO layer. All the detailed information is gathered in table 2.4. The pictures of the samples with LTO-coated LNMO layer made through ESP were shown in Figure 2.5.

Table 2. 4 Electrospray parameters for making LTO layer

Parameter	Value
Precursor concentration	0.1mol/L
Temperature	415℃
Voltage	8-10kV
Inner diameter of nozzle	0.1mm
Distance between nozzle to substrate	2.5cm
Flow rate	0.4ml/h
Spray volume	0.01ml
Spray time	1min
Annealing temperature	450℃
Annealing time	1h

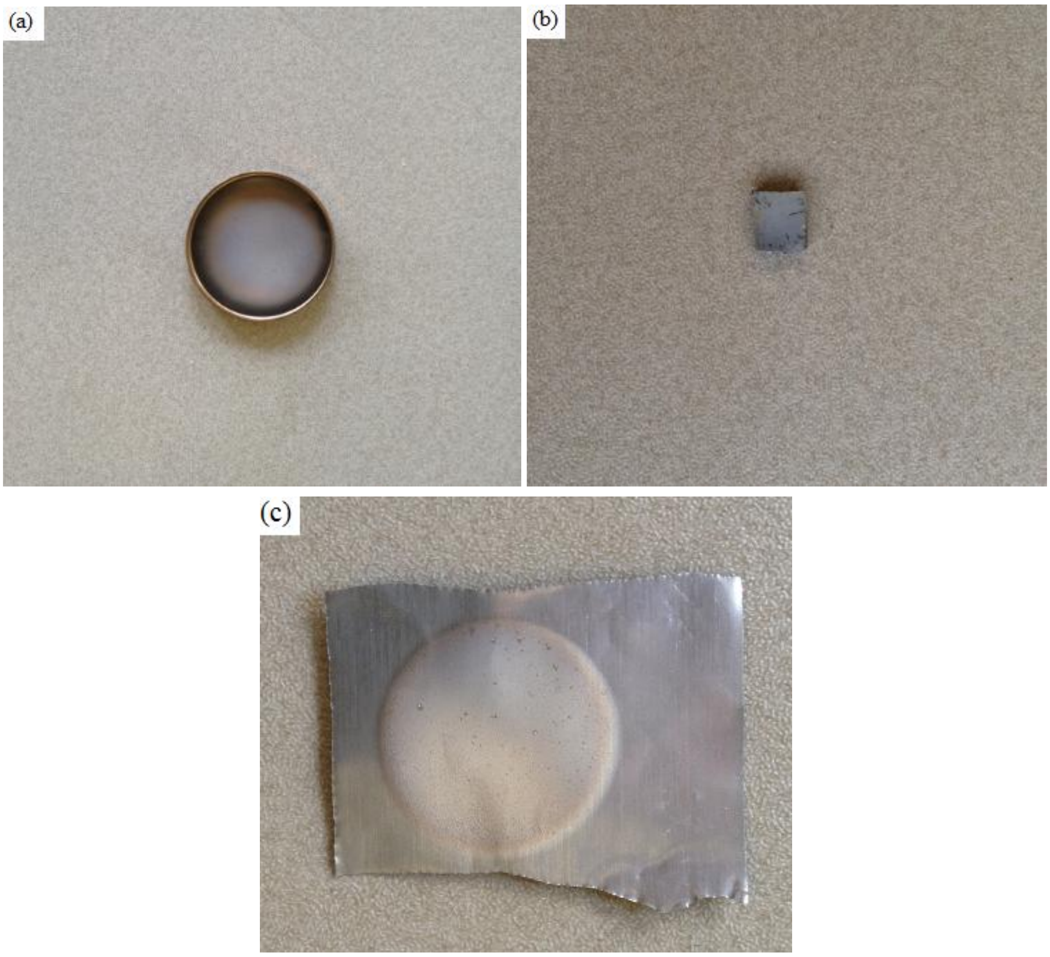

Figure 2. 5 CR2320 coin cell cap (a), gold-coated silicon wafer (b) and aluminium (c) with a LNMO layer and a LTO coating layer

2.3 Characterization methods

The charge-discharge cyclic test was done by a MACCOR multifunction Series 4000 automated test system with a charge/discharge rate of 0.1C and a upper voltage limit of 5V.

The morphology, particle sizes and thickness of the films have been investigated using a JEOL JSM 6010LA scanning electron microscope (SEM) equipped with energy dispersive X-ray spectroscopy (EDS) detector. All the samples were kept in the oven overnight before testing.

The Atomic force microscope (AFM) used in this research is an NT-MDT Ntegra platform P9, controlled by Nova px software. It was planned to do an in-situ electrochemical measurement by using a electrochemical cell setup. However, this hadn't been done due to the limitation of the engineering conditions and the schedule arrangement of the project. Instead, it was only used to investigate the morphology of the LTO-coated LNMO films and LNMO films that directly deposited on the CR2320 cell caps and the gold-coated silicon wafers.

An over view of all the testing instrument and equipment used in this project are listed in table 2.5.

Table 2. 5 Instruments used in this project

Instrument/equipment	Model
Scanning electron microscope	JEOL JSM 6010LA
Atomic force microscope	NT-MDT Ntegra platform P9
Cycler	MACCOR S4000
Energy Dispersive X-ray Spectroscopy	JEOL JSM 6010LA
Auto fine coater	JEOL JFC-1300

2.3.1 X-ray diffraction

In the test, X-ray diffraction (XRD) using a Bruker (AXS D8 Advance) X-ray diffractometer with a Cu-K_α radiation source (α=1.5418Å) in a Bragg-Brentano θ/2θ configuration. X-rays incidence from the source to the sample which is fixed in the sample stage. The diffraction angle (2θ) will vary from 0 ° to 90 ° by changing the positions of the source and the detector controlled by a computer. Then, a spectrum figure which contains the information of the planes in a certain crystal structure can be obtained. Comparing the peaks' positions with standards, the crystal structure of the sample can be identified. A schematic drawing of the instrument is shown below[78].

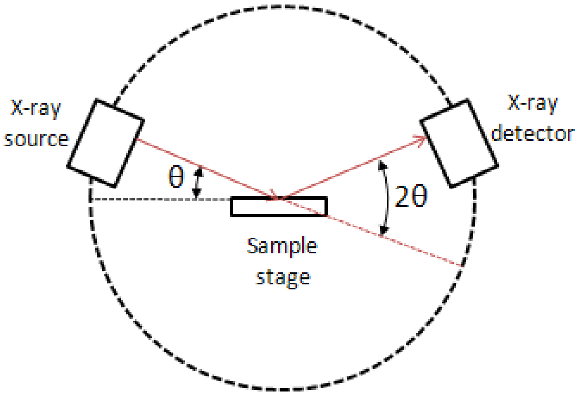

Figure 2. 6 A schematic drawing of XRD test[78]

2.3.2 Charge-discharge cyclic tests

Before starting the cyclic test, the coin cells need to be assembled in an Ar filled glove box. The CR2320 can with a LTO-coated LNMO film was as the cathode assembled into the coin cell. No additives (i.e. binders or conductivity enhancers) were used for the electrode preparation. A polyethylene membrane was used as the separator between the cathode and electrolyte. It should be wetted by few drops of 1 M $LiPF_6$ in ethylene carbonate/dimethyl carbonate (2:1) which was used as electrolyte. Other parts such as a plastic sealing ring, a lithium metal anode and a spring were stacked in the order as shown in Figure 2.7. The cell assembly process was finished after a cover was pressed properly.

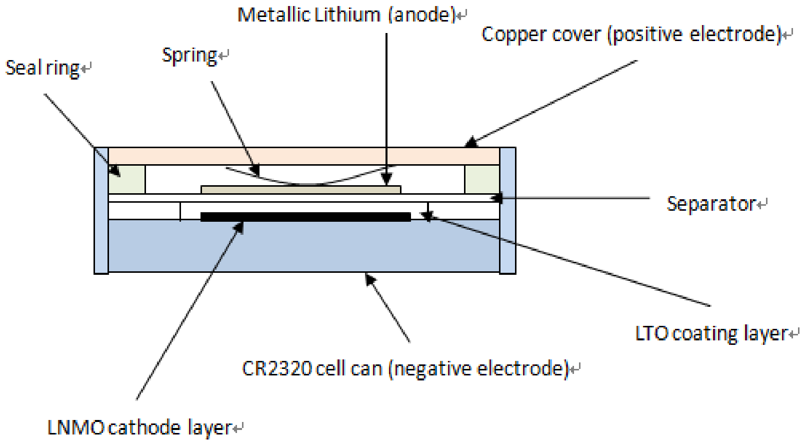

Figure 2. 7 The structure of the assembled coin cell

Samples with aluminium substrate were assembled into Swagelok cells. A photograph of the Swagelok cell is illustrated in Figure 2.8.

Figure 2. 8 Swagelok cell

2.3.3 Scanning electron microscopy

In this project, a JEOL JSM 6010LA scanning electron microscope was used in order to investigate the surface topography, the thickness of the deposited layer and the element distribution of the samples. Secondary electron imaging (SEI) and back scattered electron imaging (BSEI) were used to achieve these goals. Pictures obtained with the detection of secondary electrons can represent the topography of the sample with a good resolution since these kind of electrons are emitted from the surface of the sample (at the depth of 50-500Å) and with very low energy (less than 50eV). Pictures given by back scattered electrons can simply show the element distribution because the intensity of the BSE signal is strongly related to the atomic weight. Based on BSE images, EDS test can be done to gain more detailed information.

In the measurement, secondary electron imaging was employed with accelerate voltage at 5kV, working distance at 10mm and electron beam spot size of 50nm at lower magnifications. When increase the magnification to higher value, the spot size was decreased in order to get a clear picture. By following these initial settings, pictures with magnification ranging 100× to 1000× were acquired. Back scattered electron imaging (BEC) was employed with accelerate voltage at 20kV.

2.3.4 Energy dispersive X-ray spectroscopy

Coupled with SEM, energy dispersive X-ray spectroscopy was used to identify the elements distribution on the deposited films. The working distance and the accelerate voltage were kept the same as they applied in BSEI process. While the electron beam spot size was increased in order to increase the value of counts per second to the range of 5000-10000. Following these parameters, all the elements existing in the sample can be identified by analyzing the spectrum image. Also, the distribution information and weight percentage of each element can be analyzed.

2.3.5 Atomic force microscopy

Atomic force microscopy(AFM) is a technique that is mainly applied to image and measure the sample surface at the nano-scale, and also can be used to measure ion transport in the electrolyte. Different from optical or electron microscope, AFM dose not need to form an image by focusing light or electron beam onto the surface, but measures a 3-D image of the sample surface with a sharp probe. One advantage of AFM is that it is very easy to see and measure the dimensions of any feature in the 3-D image by using the software[79].

In this project, AFM was only used to test the morphology of the samples in a semi-contact mode in the air. The AFM used in this research is an NT-MDT Ntegra platform P9, controlled by Nova px software. The AFM probes used were the type of HA_NC, which can be applied for topography and phase imaging. These probes are fabricated by NT-MDT meant for non contact. Each of them consists of a silicon body, a polysilicon lever and silicon high resolution tip. The chip sizes are 3.6 x 1.6 x 0.45 mm. The tips are 9-16μm high and have a typical curvature radius of 10 nm. Two probes with different resonant frequencies (235±10%kHz/140±10%kHz) were connected to the edges of a rectangular cantilever. The cantilever has different dimensions on each sides. For the side connected to the probe with higher resonant frequency is 80±5μm×32±5μm ×1.7-1.8μm and for the other side is 110±5μm×32±5μm×1.7-1.8μm. In atomic force microscopy process, this cantilever was fixed into a standard AFM head and controlled by the software in semi-contact mode to sweep samples in air. Detailed information of the HA_NC probe is shown in Table 2.6[80].

Table 2. 6 Specification of HA_NC probe series[80]

Material	Polysilicon lever, monocrystal silicon tip
Chip size	3.6 x 1.6 x 0.4 mm
Reflective side	Au
Cantilever number	2 rectangular
Tip shape	Octahedral at the base, conic on the last 200 nm
Tip cone angle φ	30 degrees on the last 200nm
Full tip height	≥10 μm
Pedestal/tip ratio	1:1
Tip curvature radius	less than 10nm

Chapter 3 Results and discussion

Followed by the initial parameter settings introduced in the previous chapter, all the samples were made through electrostatic spray pyrolysis and then tested by the advanced instruments, including SEM, AFM, XRD and charge-discharge cyclic test. In this chapter, the results obtained from all these testing instruments were presented and the possible mechanisms were discussed.

3.1 Film morphology

The texture, morphology, thickness and uniformity of the samples (LNMO cathode layer with or without LTO coating) were investigated by SEM and AFM. All the samples were made through the ESP process following the fixed parameters mentioned in chapter 2. In this part, one sample with LNMO layer and one with LTO-coated LNMO layer that directly sprayed on stainless steel cap were selected for the tests.

3.1.1 LNMO layer

The LNMO cathode layer was deposited on the stainless steel cap through ESP. The precursor was sprayed onto substrate automatically controlled by the system and then followed by an annealing process. It can be seen from the AFM images (Figure 3.1a and b) that the surface texture was consisted of spherical particles with an average diameter of 100nm, approximately. These spherical particles were formed due to the characteristics of deposition technology. The charged droplets which contain the precursor solvent are dispersed in the electric field and sprayed to the heated substrate. The solvent will evaporate leaving the solute to crystalline soon after the droplets reach the heated substrate. The crystallization continues to take place when more droplets arrive on the surface of the substrate or the earlier formed particles forming a thin film with an amount of aggregates.

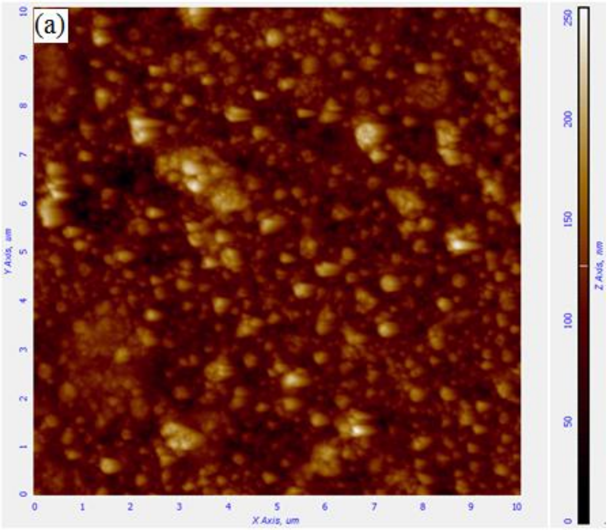

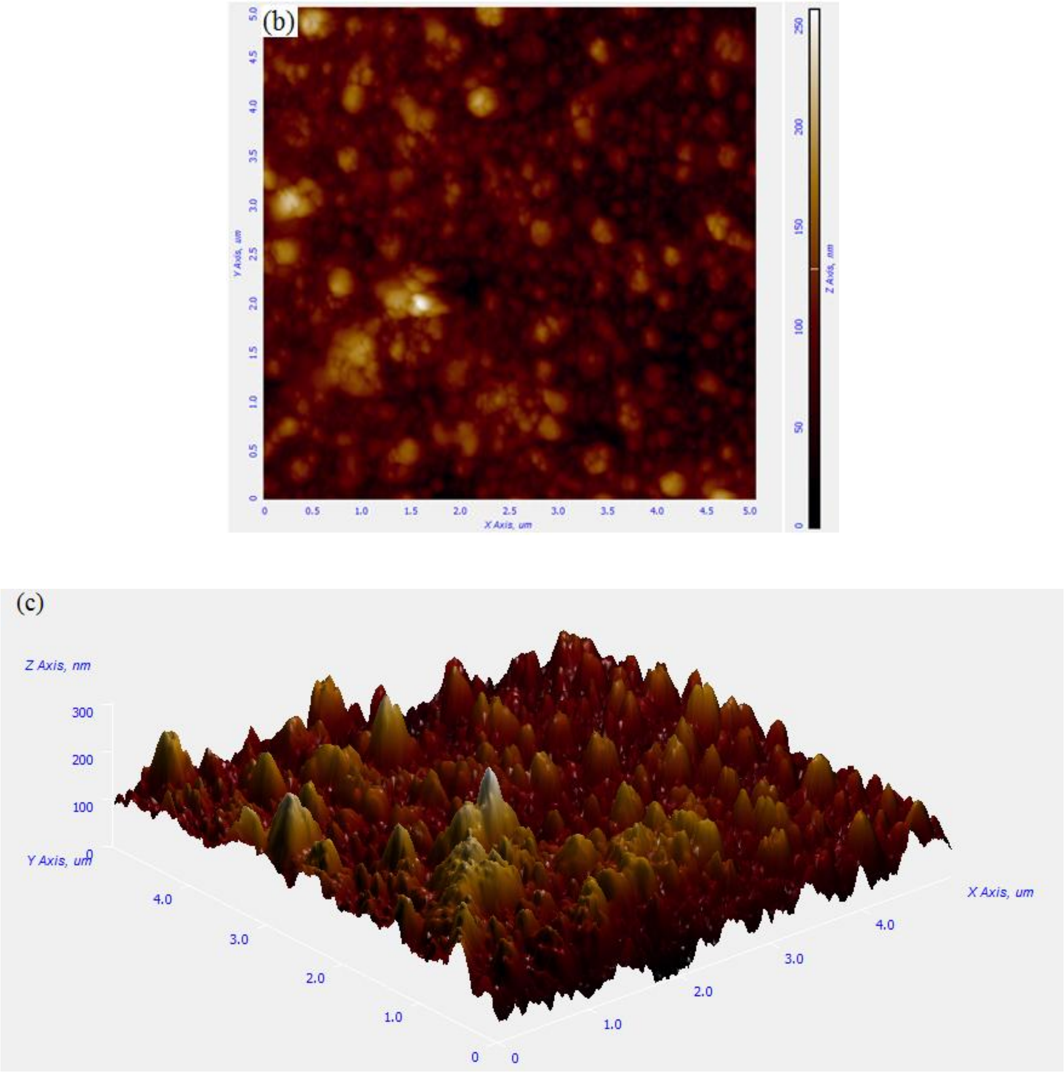

Figure 3. 1 AFM images of LNMO layer sprayed on stainless steel

It can be indicated from the 3D AFM image (Figure 3.1c) that the average thickness of the LNMO layer is around 200nm. The thickness of the film can be influenced by the initial parameters, such as precursor concentration and flow rate. The spraying time still can make a difference on thickness at the early spray stage, although it was proven by Garcia-Tamoyo[81] that the longer spraying time didn't play a significant role in increasing the thickness when it grows to several micrometers.

It also can be seen from the SEM images (Figure 3.2) that most areas of the sample surface are homogenous except few particles with the size of several micrometers exist. These big particles are probably the contaminants which might be introduced by the thickness measuring process in the laboratory. At a higher magnification, it clearly shows that those particles are not part of the homogenous layer and may come from outside. This was verified by the back scattered electron image and the followed EDS test. It can be seen from Figure 3.3a that a dark area with around 3μm was observed. Further, from the spot analysis results (Figure 3.3a and Table 3.1), it can be found that the dark area (spot 002) has a small amount of K-α signals of Ca, which are not reasonable to be present in this sample. Also, the mass percentage of C in the dark area is higher than that in the bright area (spot 003). Hence, it can be convinced that the dark spot is caused by a dust, which might be calcium carbonate. The EDS map images also proved that a thin layer was existed because both Mn and Ni elements are homogenously distributed throughout the sample surface (Figure 3.3b and c).

The secondary electron images with higher magnifications (Figure 3.2c and d) also show that a number of dark spots distributed over the scanned area. However, these dark spots have never been observed when the thickness of the deposited LNMO layer grows to several micrometers. In order to find the reasons, an other SEM test for a blank stainless steel substrate had been done. Figure 3.4 shows that a number of holes distributed at the surface of the stainless steel substrate. This could be the reason for the appearance of the dark spots. Because the deposited cathode layer was nano-scale thin and it can follow the morphology of the substrate[82]. However, when the deposited film grows to several micrometers, those small holes will be filled with later arrived droplets so that the dark spots in SEM images will become vague or even disappear. Hence, it is clear that those dark spots observed are mainly due to the surface feature of the substrate material and the thickness of the deposited film.

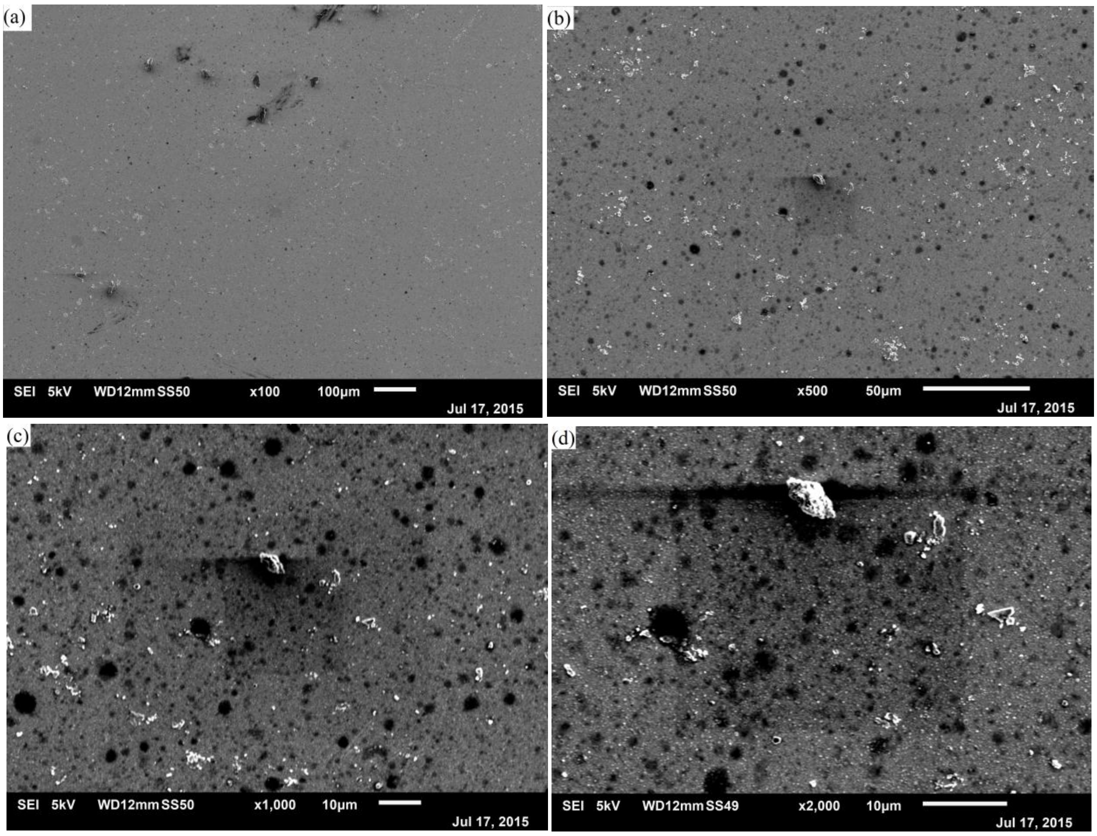

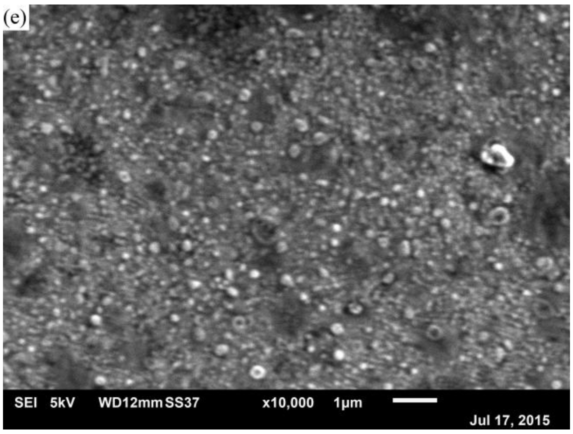

Figure 3. 2 SEI images of LNMO layer with different magnifications

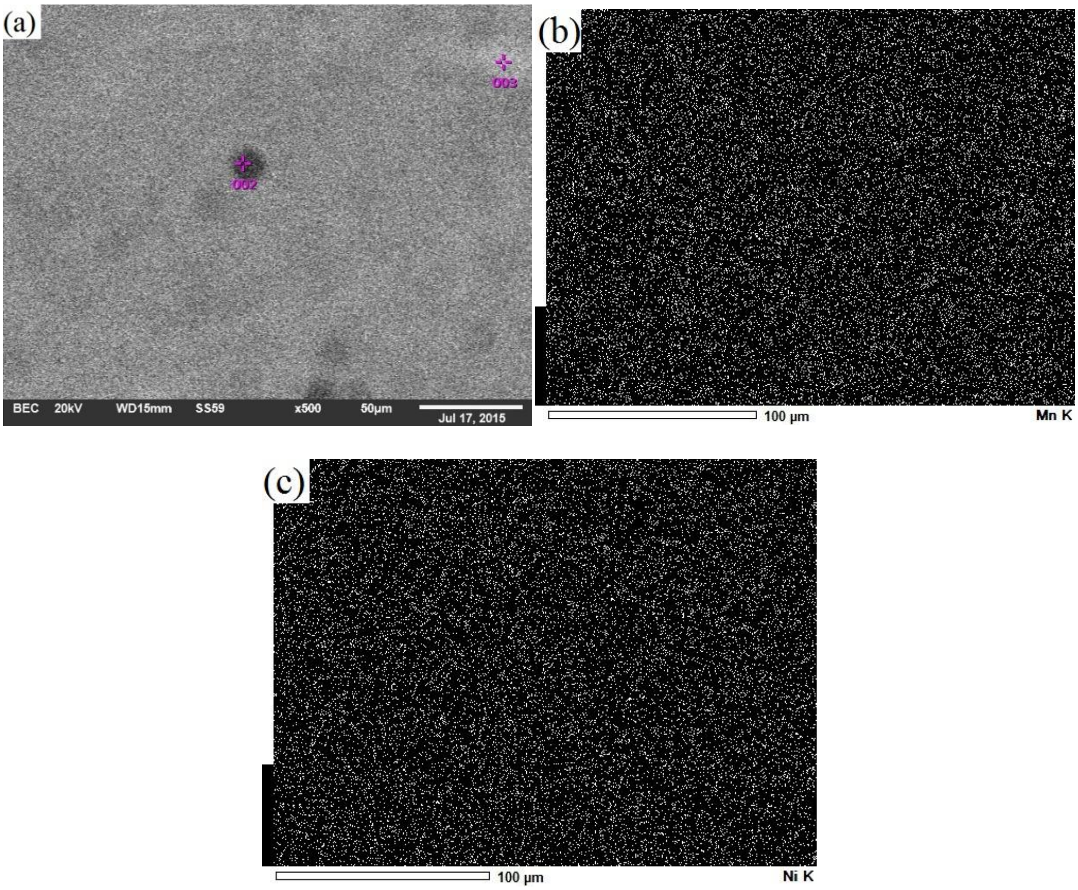

Figure 3. 3 EDS test results of LNMO layer

Table 3. 1 Spot analysis results of LNMO layer

Point 002 in Figure 3.3 a							
Chemical formula		mass%	Atom%	Sigma	Net	K ratio	Line
	C*	15.12	41.96	0.04	10392	0.0085210	K
	O*	4.38	9.12	0.06	11238	0.0312930	K
	Si*	0.39	0.47	0.03	2940	0.0029415	K
	Ca*	0.67	0.56	0.03	6276	0.0098550	K
	Cr*	15.92	10.20	0.09	84779	0.2255451	K
	Mn*	0.61	0.37	0.06	2500	0.0077072	K
	Fe*	55.56	33.15	0.15	196643	0.7012643	K
	Ni*	7.33	4.16	0.09	17412	0.0873256	K
	Total	100.00	100.00				
Point 003 in Figure 3.3 a							
Chemical formula		mass%	Atom%	Sigma	Net	K ratio	Line
	C*	6.48	22.33	0.03	4014	0.0032910	K
	O*	3.96	10.25	0.05	11682	0.0325290	K
	Si*	0.50	0.74	0.04	3428	0.0034293	K
	Cr*	17.50	13.93	0.09	88485	0.2354038	K
	Mn*	0.60	0.45	0.07	2315	0.0071372	K
	Fe*	62.72	46.49	0.17	209472	0.7470154	K
	Ni*	8.24	5.81	0.10	18345	0.0920017	K
	Total	100.00	100.00				

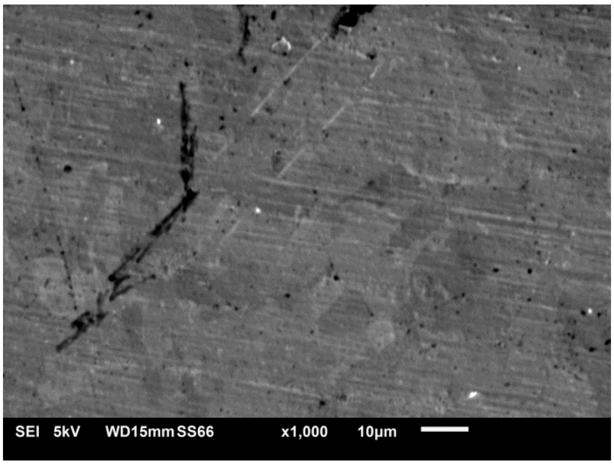

Figure 3. 4 SEI images of stainless steel substrate

3.1.2 LTO-coated LNMO layer

The LTO coating was formed on the earlier deposited LNMO layer through ESP. The initial parameters of ESP process were shown in section 2.2.5. The morphology of the sample were investigated by SEM and AFM. The AFM results (Figure 3.5 a and b) showed that the numerous aggregates of the sprayed particles are distributed homogenously. The average size of the particles is around 100nm according to the measurements by the software. This size can be influenced by the annealing temperature and time in the sample preparation steps. The aggregates could be formed by the overlapped precursor droplets during the spray process. The 3D AFM image (Figure 3.5c) showed the information on the height difference of the sample surface. It also revealed the rough morphology caused by the ESP process. It can be indicated that the thickness of the as-sprayed coating ranges from 200-600nm in an area of 5×5μm^2.

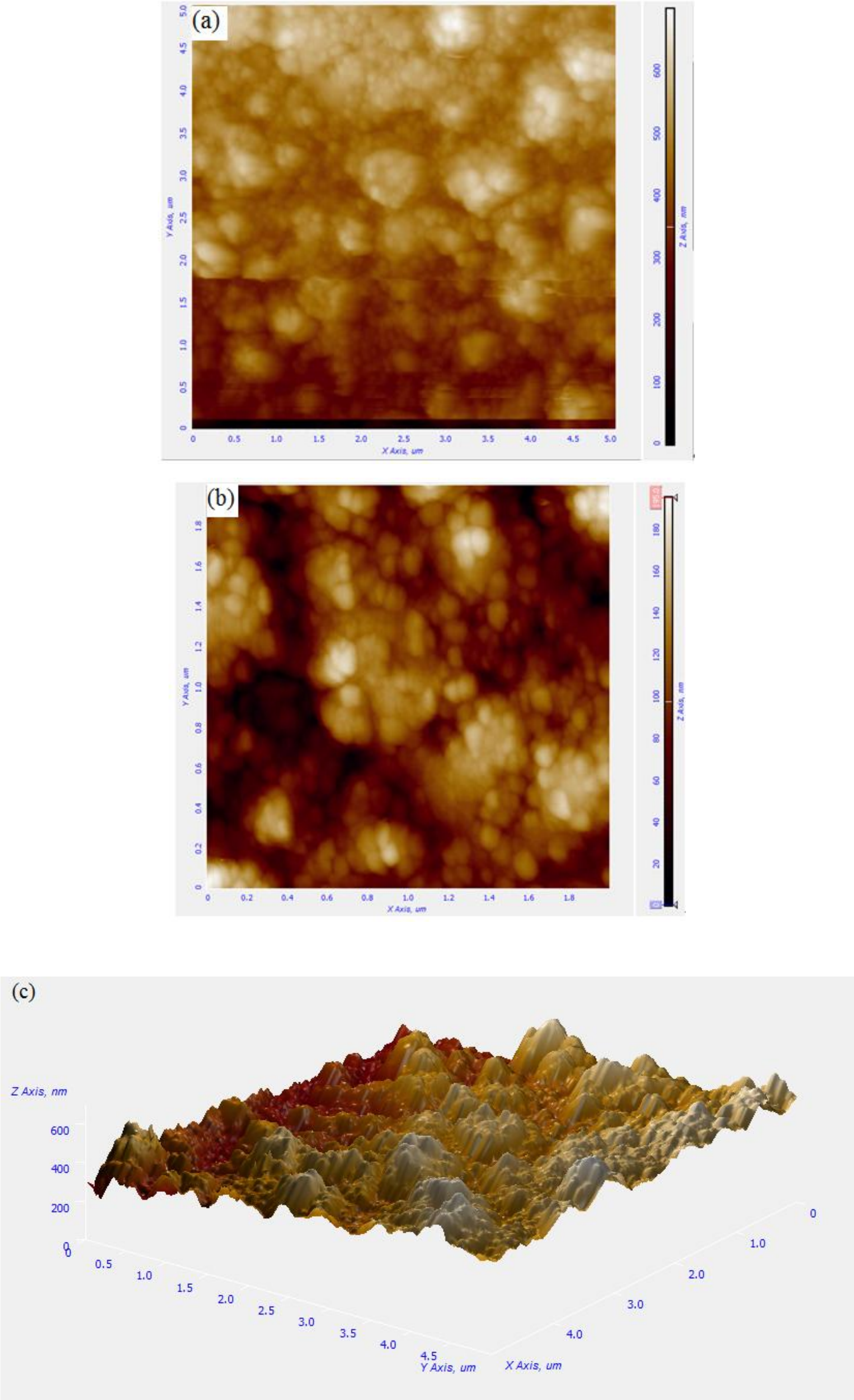

Figure 3. 5 AFM images of LTO-coated LNMO layer on stainless steel

As it can be seen in the SEM images (Figure 3.6), the typical surface texture caused by ESP was formed. The island-like particles, which could be the aggregates observed in AFM images, were homogenously distributed over the sample surface. It can be indicated that the coating might not completely cover the LNMO layer by using the initial parameters in the ESP process or those island-like particles are formed by the later arrived precursor droplets due to the suddenly increased annealing temperature when it stopped spraying. Based on these hypothesis, the back scattered electron image and the followed EDS test had been done. In the BSE images(Figure 3.7a), the dark area observed could be in result of the reflection signal of the island-like particles observed in the secondary electron images, while the bright area could be the substrate or the earlier formed layer. The results of spot analysis could be a reasonable evidence to support the deduction since the mass percentage of titanium and iron are different between these two areas. It can be seen form Table 3.2 that the mass percentage of titanium in the dark area(spot 002) is higher than that in the bright area (spot 003). On the other hand, that value of iron in the dark area is smaller than that in the bright area. Further more, it can be seen from the EDS map images (Figure 3.7b) that more Ti signals were generated at the place corresponding to the dark area in Figure 3.7a. Meanwhile, Ti, Mn and Ni elements are all homogenously distributed over the sample surface(Figure 3.7b, c and d). Above all, it can be concluded that a very thin coating was formed on the earlier sprayed LNMO layer. The average thickness of this coating is around 400nm. However, the crystal structures of the both layers remain unknown. They need to be investigated by XRD tests.

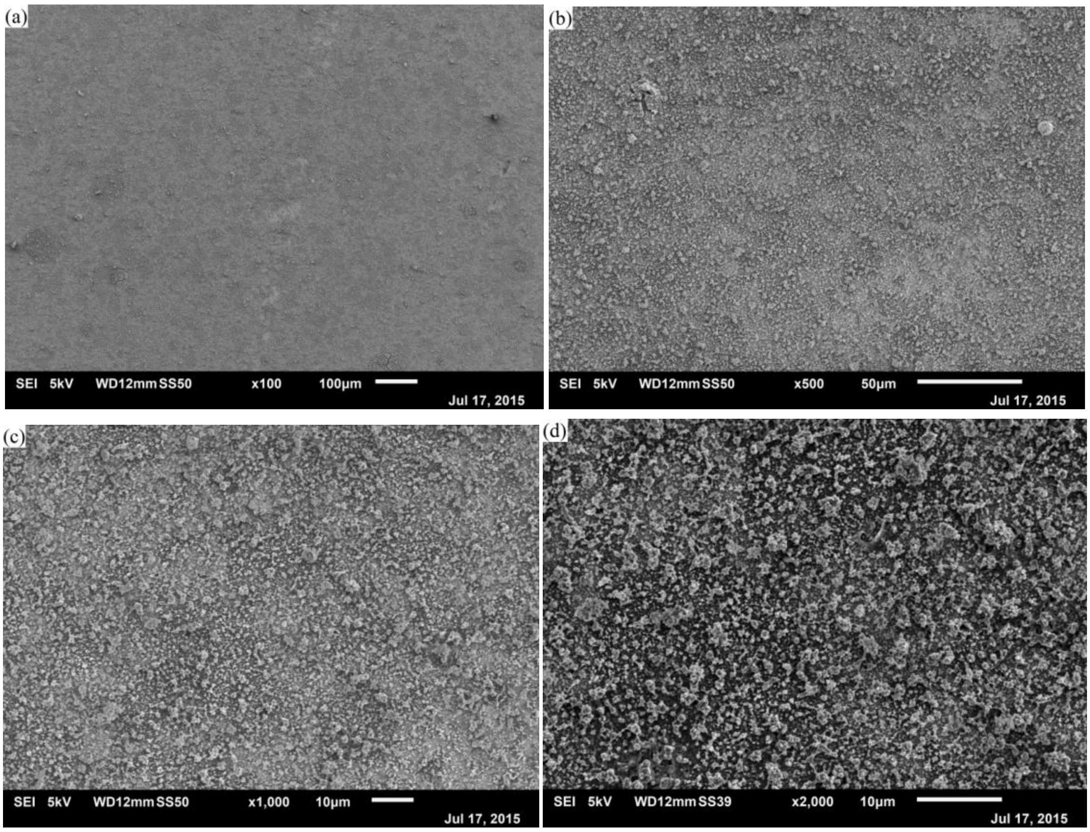

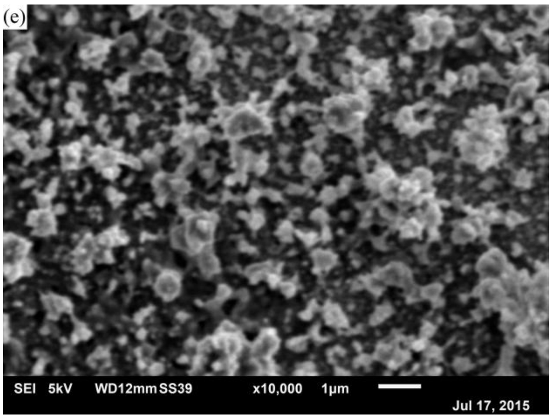

Figure 3. 6 SEI images of coated LNMO layer with different magnifications

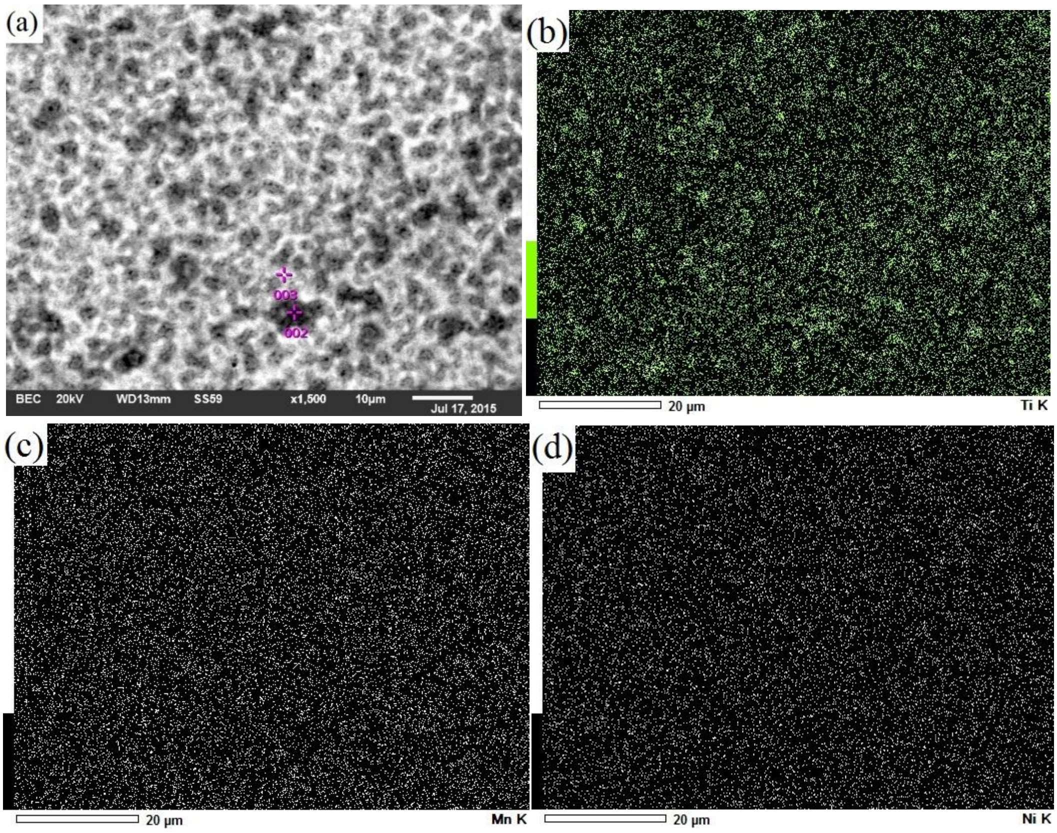

Figure 3. 7 EDS map information of coated LNMO layer

Table 3. 2 Spot analysis of coated LNMO layer

Point 002 in Figure 3.6 a							
Chemical formula		mass%	Atom%	Sigma	Net	K ratio	Line
	C*	8.80	24.03	0.03	6539	0.0053614	K
	O*	14.19	29.09	0.07	27684	0.0770869	K
	Ti*	12.48	8.55	0.06	79172	0.1631118	K
	Cr*	13.47	8.50	0.08	66746	0.1775699	K
	Mn*	1.47	0.88	0.06	5857	0.0180582	K
	Fe*	43.72	25.68	0.14	151557	0.5404804	K
	Ni*	5.88	3.28	0.09	13964	0.0700329	K
	Total	100.00	100.00				
Point 003 in Figure 3.6 a							
Chemical formula		mass%	Atom%	Sigma	Net	K ratio	Line
	C*	6.35	20.05	0.03	4454	0.0036523	K
	O*	9.07	21.50	0.05	25170	0.0700860	K
	Ti*	4.09	3.23	0.04	26727	0.0550641	K
	Cr*	16.22	11.82	0.09	86131	0.2291401	K
	Mn*	1.46	1.00	0.06	6054	0.0186646	K
	Fe*	55.54	37.70	0.15	198972	0.7095715	K
	Ni*	7.27	4.69	0.09	17524	0.0878864	K
	Total	100.00	100.00				

3.2 Electrochemical behavior

The LNMO cathode layer and the coating layer that directly deposited on various substrates were assembled into coin cells and Swagelok cells for the charge-discharge cyclic test. Figure 3.8b shows the galvanostatic charge-discharge curve of the coating layer. It can be found that this curve doesn't give any information of LTO since the voltage linearly changing from 2.2V to 0.8V, approximately. A typical curve of LTO (Figure 3.8a) has a plateau at 1.55V, which is caused by the insertion or extraction process of lithium ions. However, according to the literature, this curve is very similar to the charge-discharge curve of nano-structured TiO_2 anatase, which can be calcined at around 400℃ (Figure 3.8c)[83-84]. But this doesn't make sense since the lithium also exist in the precursor solution. Based on the precursor stoichiometry, the coating is probably consisted of amorphous lithium-titanium oxides, which lead to the slope curve in Figure 3.8b.

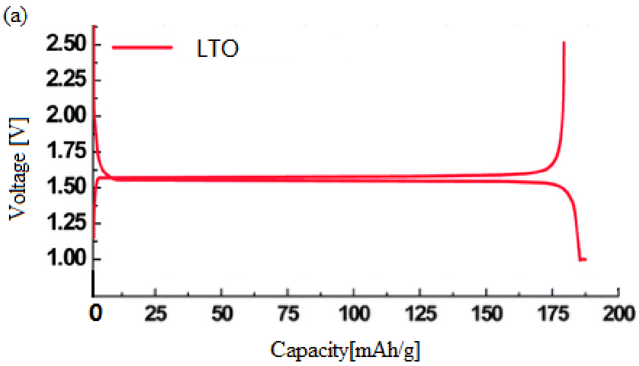

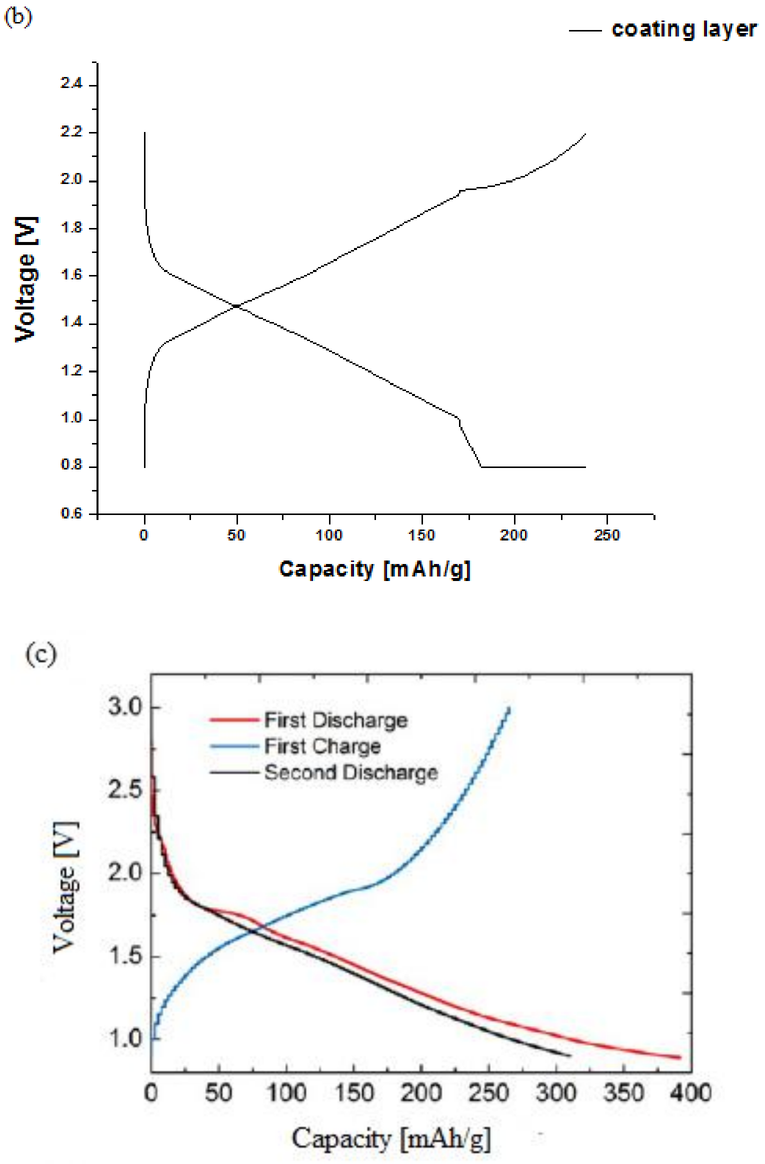

Figure 3. 8 Galvanostatic charge-discharge curve of a typical LTO (a), the coating layer (b) and the nano-structured TiO_2 anatase (c) [82-83].

The reason is probably due to the relatively lower heating temperature and annealing temperature which were set to be 415℃ and 450℃, respectively. According to Yu's research, a spinel LTO was successfully deposited on platinum substrate by electrostatic spray deposition after annealed at a range of 650-850℃ for 2 hours[85]. Also, Li's research suggested that an epitaxial LTO coating can be formed at around 700°C by sol-gel reaction[86]. Hence, it is reasonable to increase the temperature and annealing time in order to form LTO. However, ESP might be not suitable for depositing LTO coating material since the deposition temperature is limited by the equipment. For instance, when the temperature is set to higher values, the morphology and the thickness of the coating will change a lot during the electrospray process.

Till now, no ideal charge-discharge curves of LNMO or coated-LNMO were obtained. One possible reason for this might be the inappropriate cell assembly process which can result in self-discharge in the cell. Another possible reason is that the spinel structure of cathode layer has not been formed during the ESP process. In order to verify these hypothesis, other characterization methods need to be applied.

3.3 Structural characterization

The crystal structures of LNMO cathode layer and the LTO coating layer were investigated by XRD. All the samples were made by ESP following the same initial parameters, including precursor concentration, spray volume, spray rate, distance between the nozzle and the substrate, voltage, temperature and annealing process. Therefore, it can be convinced that similar crystal structures were formed on different substrate materials. For this reason, samples with aluminium substrate were selected for XRD tests as they are easier to be fixed into the holder in the instruments.

Till now, this test has not been done yet due to the time restrictions and the instrument maintenance. Hopefully, it will be done before the presentation. Then, the results will be shown during the final presentation.

Chapter 4 Conclusion and Recommendation

In this project, a nano-scale thin and homogenous Lithium titanate-coated LNMO layer has been successfully deposited on various substrates by electrostatic spray pyrolysis process. The average thickness of LNMO and the coating layer are around 200nm and 400nm, respectively.

Unfortunately, the analysis of the electrochemical properties of this coated LNMO was failed. No charge-discharge curves have been successfully measured. The possible reasons leading to this poor result can be attributed to different aspects. For instance, the spinel structure of cathode layer has not been formed during the ESP process, or the cell was not well assembled so that self-discharge happened.

In addition, the cyclic test of the coating layer reveals that LTO was failed to be formed. The deposited coating is more likely to be an amorphous lithium-titanium oxide which gives a slope charge-discharge curve. In order to form a pure LTO spinel structure, the temperature may need to rise to above 600°C. However, ESP might be not suitable for depositing LTO coating material since the deposition temperature is limited by the equipment.

The crystal structures of both layers need to be identified by XRD. According to the former results, the cathode layer which were made from the same precursor by ESP but with thickness as several micrometers formed the spinel structure. Hence, it can be expected that the thinner cathode layer which were made through the same process will probably form the spinel structure as well. However, it might be difficult to see the Bragg peaks in XRD pattern since the deposited layers are nano-scale thin and the average crystallite size is small caused by the relatively lower annealing temperature.

In future work, an effective method for depositing LTO needs to be found. After that, more characterization methods can be utilized to study other properties. For instance, AFM can be modified to measure the in-situ characterization of lithium ion transfer at/from the electrode surface.

Acknowledgement

People are different. I believe that every Chinese student had their different experiences, goals and understandings before they came to this beautiful city located in South Holland. But I do still remember how I felt at the first day when I arrived in Delft. I was a freshman with little luggage and less communication skills in English and even less experience of living aboard. What I had at that time, and still have at present, is a faithful heart that wanted to learn the true scientific knowledge and to know the world. I am always waiting for a chance to express my gratefulness to those people whom helped me directly or indirectly during those two years. Now it is the chance to say this.

First of all, I want to show my appreciates to TU/Delft and the people who work or study in this great university. Because you create such a great academic atmosphere that allows me to go deep into the theories which I wanted to know. It is your strict education attitude and your systematical teamwork that make me become a more confident man who would like to take more responsibilities in the future. It is also your names, your faces and your spirits that consist of the special memory of mine in the recent two years. I should treasure all of you.

Then, I would like to give the special thanks to my supervisor Dr. Erik Kelder. During the year that I spent at the office 1.017 in ChemE, I am very appreciated for the unconditional help that you gave me every time when I came to you no matter how busy you were. The words you said about the way to do scientific researches taught me a lot. I am very lucky to do this master thesis in your group.

I also would like to say thanks very much to my daily supervisor Raphaël Fredon. You helped me a lot from the trivial matters in daily life to the difficulties in scientific researches. I can not done these all by myself since I had little knowledge about batteries and also the laboratory regulations in the first few months. You are a kind man and a good buddy. Wish you all the best in the future!

I am also glad to give my thanks to the other committee members: Prof.Ernst Sudhölter and Dr.Ir.Marnix Wagemaker. Thanks for accepting my invitation and your attendance. It is my honor to share this important day with you.

Thanks also go to the technicians. It is impossible for me to finish this thesis without your sincere suggestions and professional trainings. I would thank Marcel and Duco for your patience and kindness help during those training lessons. I am also appreciated for the scientific knowledge that you delivered to me.

Also, I feel good to work with my colleagues in 1.017 in ChemE. Thanks to Frans, Miguel, Sheila, Pierre, Elise, BoKai, Frieda and Kirsten for your help from many aspects. Special thanks to Frans for your kind help and sincere suggestions in the electrospray process and cyclic test. I appreciate with your optimistic attitude towards the things in life and in researches since that encouraged me when the difficulties came.

I am also grateful to my roommates in Rotterdamseweg 139A-22 and all the other friends in Delft and in China. I will remember those happy hours with you guys since those moments helped me to overcome lonely and lost.

In the end, I would give my love to my mother, father, aunt and other family members. I can not go this far without your support. I miss all of you.

References

[1] UNEP (2013) Metal Recycling: Opportunities, Limits, Infrastructure, A Report of the Working Group on the Global Metal Flows to the International Resource Panel. Reuter, M. A.; Hudson, C.; van Schaik, A.; Heiskanen, K.; Meskers, C.; Hagelüken, C.

[2] Renewable energy, available at: https://en.wikipedia.org/wiki/Renewable_energy (accessed 1 August 2015).

[3] David, M. (2009) Sustainable Energy — without the hot air. United Kingdom: UIT Cambridge Ltd.

[4] UNEP (2013) Metal Recycling: Opportunities, Limits, Infrastructure, A Report of the Working Group on the Global Metal Flows to the International Resource Panel. Reuter, M. A.; Hudson, C.; van Schaik, A.; Heiskanen, K.; Meskers, C.; Hagelüken, C.

[5] UNEP (2013) Metal Recycling: Opportunities, Limits, Infrastructure, A Report of the Working Group on the Global Metal Flows to the International Resource Panel. Reuter, M. A.; Hudson, C.; van Schaik, A.; Heiskanen, K.; Meskers, C.; Hagelüken, C.

[6] Bruno, S. (2011) 'History of lithium batteries', Solid State Electrochem, vol. 15, pp. 1623-1630.

[7] Bruno, S. (2011) 'History of lithium batteries', Solid State Electrochem, vol. 15, pp. 1623-1630.

[8] WHITTINGHAM, M.S.. (1976) 'Electrical Energy Storage and Intercalation Chemistry', SCIENCE, vol. 192, pp. 1126-1127.

[9] Lithium-ion battery, available at: https://en.wikipedia.org/wiki/Lithium-ion_battery (accessed 1 August 2015).

[10] What is the best battery, available at: http://batteryuniversity.com/learn/article/whats_the_best_battery (accessed 1 August 2015).

[11] Bruno, S. (2011) 'History of lithium batteries', Solid State Electrochem, vol. 15, pp. 1623-1630.

[12] J.M, Tarascon and M, Armand. (2001) 'Issues and challenges facing rechargeable lithium batteries', Nature, Vol. 414, pp. 359-367.

[13] The Rocking Chair Battery (Lithium Ion Battery), available at: https://physicsandsocietybc.wordpress.com/2013/04/03/the-rocking-chair-battery-lithium-ion-battery/ (accessed 1 August 2015).

[14] Nagaura T., and Tazawa K., 1990. Lithium ion rechargeable battery, Japan. Prog. Batteries sol. Cells, 9: 209–210.

[15] John, B., G and Kyu-Sung, P. (2013) 'The Li-Ion Rechargeable Battery: A Perspective', American Chemical Society, Vol. 135, pp. 1167-1176.

[16] Advantages & Limitations of the Lithium-ion Battery, available at: http://batteryuniversity.com/learn/article/is_lithium_ion_the_ideal_battery (accessed 1 August 2015).

[17] Jie, Z., Rui, W. and Xiaocheng, Y. (2012) 'Direct Observation of Inhomogeneous Solid Electrolyte Interphase on MnO Anode with Atomic Force Microscopy and Spectroscopy',

American Chemical Society, vol. 12, pp. 2153–2157.

[18] Andrew, R and Wilmont, H. (2006) 'Recent developments and likely advances in lithium-ion batteries', Journal of Power Sources, vol. 162, pp. 809-812.

[19] Michel, and Graham, A. (2004) 'Li-ion batteries and portable power source prospects for the next 5–10 years', Journal of Power Sources, vol. 136, pp. 386-394.

[20] Michel, A., Frank, E and Douglas R. M. (2009) 'ionic-liquid materials for the electrochemical challenges of the future', Nature materials, vol. 8, pp. 621-629.

[21] Joon-Ho, S., Wesley, H and Stefano, P. (2005) 'PEO-Based Polymer Electrolytes with Ionic Liquids and Their Use in Lithium Metal-Polymer Electrolyte Batteries', J. Electrochem. Soc, vol. 152, pp. A978-A983.

[22] D, Singh., W.S Kima and V. Craciuna. (2002) 'Microstructural and electrochemical properties of lithium manganese oxide thin films grown by pulsed laser deposition', Appl. Surf. Sci, vol. 197, pp. 516-521.

[23] A. K., Padhi., K. S. Nanjundaswamy and J. B. Goodenough. (1997) 'Phospho-olivines as Positive-Electrode Materials for Rechargeable Lithium Batteries', J. Electrochem. Soc, vol. 144, pp. 1188-1193.

[24] Yan, Z., Yongguang, Z and Denise, G. (2012) 'Polymer Electrolytes for Lithium/Sulfur Batteries', Membranes, vol. 2, pp.553-564.

[25] Lee, E and Persson, K. (2013) 'First-principles study of the nano-scaling effect on the electrochemical behavior in $LiNi_{0.5}Mn_{1.5}O_4$', Nanotechnology, vol. 24, pp. 288-296.

[26] Guoqiang, L. (2012) '$LiNi_{0.5}Mn_{1.5}O_4$ Spinel and Its Derivatives as Cathodes for Li-Ion Batteries', InTech, Available at: http://www.intechopen.com/books/lithium-ion-batteries-new-developments/spinel-lini0-5mn1-5o4-and-itsderivatives-as-cathodes-for-li-ion-batteries (accessed 1 August 2015).

[27] Jianqiu, D., Zhouguang, L. and I. Belharouak. (2009) 'Preparation and electrochemical properties of $Li_4Ti_5O_{12}$ thin film electrodes by pulsed laser deposition', Journal of Power Sources, vol. 193, pp. 816 – 821.

[28] Guoqiang, L. (2012) '$LiNi_{0.5}Mn_{1.5}O_4$ Spinel and Its Derivatives as Cathodes for Li-Ion Batteries', InTech, Available at: http://www.intechopen.com/books/lithium-ion-batteries-new-developments/spinel-lini0-5mn1-5o4-and-itsderivatives-as-cathodes-for-li-ion-batteries (accessed 1 August 2015).

[29] Jili, L., Youqi, Z and Lin W. (2014) 'Lithium Titanate Epitaxial Coating on Spinel Lithium Manganese Oxide Surface for Improving the Performance of Lithium Storage Capability', American Chemical Society, vol. 6, pp. 18742−18750.

[30] Santhanam, R. and Rambabu, B. (2010) 'Research progress in high voltage spinel LiNi0.5Mn1.5O4 material', Journal of Power Sources, vol. 195, pp. 5442 – 5451.

[31] Sun, Y.-K., Hong, K.-J. and Prakash, J. (2002) 'Electrochemical performance of nano-sized ZnO-coated LiNi0:5Mn1:5O4 spinel as 5 V materials at elevated temperatures', Electrochemistry Communications, vol. 4, pp. 344-348.

[32] Yukai, F, Jianming, W and Zheng, T. (2007) 'Effects of the nanostructured SiO2 coating on the performance of $LiNi_{0.5}Mn_{1.5}O_4$ cathode materials for high-voltage Li-ion batteries', Electrocheimica Acta, Vol. 52, pp. 3870-3875.

[33] Esteban, G.T. (2014) 'Advanced Thin Layer Deposition of Materials for Li-ion Batteries via Electrospray'. A thesis submitted in partial fulfilment of the Requirements of Technical

University of Delft for the Degree of Doctor of Philosophy. Delft: Technical University of Delft.

[34] Jianqiu, D., Zhouguang, L. and I. Belharouak. (2009) ‘Preparation and electrochemical properties of $Li_4Ti_5O_{12}$ thin film electrodes by pulsed laser deposition’, Journal of Power Sources, vol. 193, pp. 816 – 821.

[35] Jie, Z., Rui, W. and Xiaocheng, Y. (2012) ‘Direct Observation of Inhomogeneous Solid Electrolyte Interphase on MnO Anode with Atomic Force Microscopy and Spectroscopy’, American Chemical Society, vol. 12, pp. 2153–2157.

[36] Kazumi, K., Tadashi, T., and Masasuke, T. (2008) ‘Mass Production and Battery Properties of $LiNi_{0.5}Mn_{1.5}O_4$ Powders Prepared by Internal Combustion Type Spray Pyrolysis’, Key Engineering Materials, vol. 388, pp. 85-88.

[37] Mukoyama, I., Myoujin, K. and Nakamura, T. (2010) ‘Mass Production of LiFeP/C Powders by Large Type Spray Pyrolysis Apparatus and Its Application to Cathode for Lithium Ion Battery’, International Journal of Chemical Engineering, vol. 208, pp. 88-93.

[38] Arrebola, J.C., Caballero, A., and Hernan, L. (2008) ‘Polymer-mediated growth of highly crystalline nano- and micro-sized LiNi0.5Mn1.5O4 spinels’, EUROPEAN JOURNAL OF INORGANIC CHEMISTRY, vol. 21, pp. 3302-3310.

[39] Arrebola, J.C., Caballero, A., and Hernan, L. (2005) ‘Adverse effect of Ag treatment on the electrochemical performance of the 5 V nanometric spinel LiNi0.5Mn1.5O4 in lithium cells’, ELECTROCHEMICAL AND SOLID-STATE LETTERS, vol. 8, pp. 303-308.

[40] Feng, J.K., Xia, H. and Lai, M.O. (2009) ‘NASICON structured LiGe2(PO4)3 with improved cyclability for high performance lithium batteries’, J. Phys. Chem. C, vol. 113, pp. 20514-20520.

[41] Porter, D.A. and Easterling, K.E. (1992) Phase Transformation in Metals and Alloys. Second edition. London: Chapman & Hall.

[42] Jili, L., Youqi, Z and Lin W. (2014) ‘Lithium Titanate Epitaxial Coating on Spinel Lithium Manganese Oxide Surface for Improving the Performance of Lithium Storage Capability’, American Chemical Society, vol. 6, pp. 18742−18750.

[43] Cho, J. (2008) ‘VOx-Coated LiMn2O4 Nanorod Clusters for Lithium Battery Cathode Materials’. J. Mater. Chem, vol. 18, pp. 2257−2261.

[44] Walz, K.A., Johnson, C.S. and Genthe, J. (2010) ‘Elevated Temperature Cycling Stability and Electrochemical Impedance of $LiMn_2O_4$ Cathodes with Nanoporous ZrO_2 and TiO_2 Coatings’. J. Power Sources, vol. 195, pp. 4943−4951.

[45] Guoqiang, L. (2012) ‘$LiNi_{0.5}Mn_{1.5}O_4$ Spinel and Its Derivatives as Cathodes for Li-Ion Batteries’, InTech, Available at: http://www.intechopen.com/books/lithium-ion-batteries-new-developments/spinel-lini0-5mn1-5o4-and-itsderivatives-as-cathodes-for-li-ion-batteries (accessed 1 August 2015).

[46] Locati, C., Lafont, U. and Simonin, L. (2007) ‘Mg-doped $LiNi_{0.5}Mn_{1.5}O_4$ spinel for cathode materials’. JOURNAL OF POWER SOURCES, vol. 174 (2), pp. 847-851.

[47] Alcántara, R., Jaraba, M. and Lavela, P. (2002) ‘NiCo2O4 Spinel: First Report on a Transition Metal Oxide for the Negative Electrode of Sodium-Ion Batteries’, Chem. Mater, vol. 14 (7), pp. 2847–2848.

[48] Park, S.B., Eom, W.S. and Cho, W.I. (2006) ‘Electrochemical properties of $LiNi_{0.5}Mn_{1.5}O_4$ cathode after Cr doping’, Journal of Power Sources, vol. 159, pp. 679-684.

[49] Liu, G.Q., Yuan, W.S. and Liu, G.Y. (2009) ‘The electrochemical properties of $LiNi_{0.5}Mn_{1.2}Ti_{0.3}O_4$

compound', Journal of Alloys and Compounds, vol. 484, pp. 567-569.

[50] Hong, K.J. and Sun, Y.S. (2002) 'Electrochemical performance of nano-sized ZnO-coated $LiNi_{0.5}Mn_{1.5}O_4$ spinel as 5 V materials at elevated temperatures', Electrochemistry Communications, vol. 4, pp. 344-348.

[51] Baggetto, L., Dudney, N.J. and Veith, G.M. (2013) 'Surface chemistry of metal oxide coated lithium manganese nickel oxide thin film cathodes studied by XPS', Electrochim. Acta, vol. 90, pp. 135–147.

[52] Yukai, F, Jianming, W and Zheng, T. (2007) 'Effects of the nanostructured SiO_2 coating on the performance of $LiNi_{0.5}Mn_{1.5}O_4$ cathode materials for high-voltage Li-ion batteries', Electrocheimica Acta, Vol. 52, pp. 3870-3875.

[53] Na, L., Guangmin, Z and Feng, L. (2013) 'A Self-Standing and Flexible Electrode of $Li_4Ti_5O_{12}$ Nanosheets with a N-Doped Carbon Coating for High Rate Lithium Ion Batteries', Advanced Functional Materials, vol. 23, pp. 5429–5435.

[54] Sun, X.C., Pavle V. and Radovanovic. (2015) 'Advances in spinel Li4Ti5O12 anode materials forlithium-ion batteries', New Journal of Chemistry, vol. 39, pp. 1-756.

[55] Zhou, X.L., Huang, R.A. and Wu, Z.C. (2010) 'Synthesis and Electrochemical Properties of High-Rate Spinel Li4Ti5Ol2/TiN Anode Material for Lithium-Ion Batteries', Acta Physico-Chimica Sinica, Vol. 26, pp. 3187-3192.

[56] Jaiswal, A. (2010) 'Nanoscale $LiFePO_4$ and $Li_4Ti_5O_{12}$ for High Rate Li-ion Batteries', Journal of the Electrochemical Society, vol. 156, pp. A1041-A1046.

[57] Guoqiang, L. (2012) '$LiNi_{0.5}Mn_{1.5}O_4$ Spinel and Its Derivatives as Cathodes for Li-Ion Batteries', InTech, Available at: http://www.intechopen.com/books/lithium-ion-batteries-new-developments/spinel-lini0-5mn1-5o4-and-itsderivatives-as-cathodes-for-li-ion-batteries (accessed 1 August 2015).

[58] Xiang, H.F., Jin, Q.Y. and Wang, R. (2008) 'Nonflammable electrolyte for 3-V lithium-ion battery with spinel materials $LiNi_{0.5}Mn_{1.5}O_4$ and $Li_4Ti_5O_{12}$', Journal of Power Sources, vol. 179, pp. 351-356.

[59] Jili, L., Youqi, Z and Lin W. (2014) 'Lithium Titanate Epitaxial Coating on Spinel Lithium Manganese Oxide Surface for Improving the Performance of Lithium Storage Capability', American Chemical Society, vol. 6, pp. 18742−18750.

[60] Tsutomu, O., Atsushi, U. and Norihiro, Y. (1995) 'Zero strain insertion material of $Li[Li_{1/3}Ti_{5/3}]O_4$ for rechargeable lithium cells', J. Electrochem. Soc. Vol. 142, pp. 1431-1435.

[61] Yi, T.F., Shu, J. and Zhu, Y.R. (2009) 'Structure and electrochemical performance of $Li_4Ti_5O_{12}$-coated $LiMn_{1.4}Ni_{0.4}Cr_{0.2}O_4$ spinel as 5 V materials', Electrochemistry Communications, vol. 11, pp. 91-94.

[62] Na, L., Guangmin, Z and Feng, L. (2013) 'A Self-Standing and Flexible Electrode of $Li_4Ti_5O_{12}$ Nanosheets with a N-Doped Carbon Coating for High Rate Lithium Ion Batteries', Advanced Functional Materials, vol. 23, pp. 5429–5435.

[63] Jili, L., Youqi, Z and Lin W. (2014) 'Lithium Titanate Epitaxial Coating on Spinel Lithium Manganese Oxide Surface for Improving the Performance of Lithium Storage Capability', American Chemical Society, vol. 6, pp. 18742−18750.

[64] Deng, H.F., Nie, P. and Luo, H.F. (2014) 'Highly enhanced lithium storage capability of $LiNi_{0.5}Mn_{1.5}O_4$ by coating with Li_2TiO_3 for Li-ion batteries', J. Mater. Chem. A , vol. 2, pp. 18256–18262.

[65] Liu,J.H., Wei, X.F. and Liu, X.W. (2015) 'Two-Dimensional Wavelike Spinel Lithium Titanate for Fast Lithium Storage',

[66] H. M, Wu., I. Belharouak and H, Deng. (2009) 'Development of $LiNi_{0.5}Mn_{1.5}O_4/Li_4Ti_5O_{12}$ System with Long Cycle Life', J. Electrochem. Soc, vol. 156, pp. A1047-A1050.

[67] Jili, L., Youqi, Z and Lin W. (2014) 'Lithium Titanate Epitaxial Coating on Spinel Lithium Manganese Oxide Surface for Improving the Performance of Lithium Storage Capability', American Chemical Society, vol. 6, pp. 18742–18750.

[68] Yu, Y., Shui, J.L. and Chen, C.H. (2005) 'Electrostatic spray deposition of spinel $Li_4Ti_5O_{12}$ thin films for rechargeable lithium batteries', Solid State Communications, vol. 135, pp. 485–489.

[69] Lin, X., Pan, F. and Wang, H. (2014) 'Progress of $Li_4Ti_5O_{12}$ anode material for lithium ion batteries', Materials A82 Technology: Advanced Functional Materials, vol. 29, pp. A82-A87.

[70] Electrospray, available at: https://en.wikipedia.org/wiki/Electrospray (accessed 1 August 2015).

[71] Esteban, G.T. (2014) 'Advanced Thin Layer Deposition of Materials for Li-ion Batteries via Electrospray'. A thesis submitted in partial fulfilment of the Requirements of Technical University of Delft for the Degree of Doctor of Philosophy. Delft: Technical University of Delft.

[72] Wuled Lenggoro, I., Okuyama, K. and Mora, J. (2000) 'Preparation of ZnS nanopartilces by electrospray pyrolysis', Journal of Aerosol Science, vol. 31, pp. 121-136.

[73] Terada, Y., Suzuki, Y. and Tohno, S. (2012) 'Synthesis and characterization of TiO_2 powders by electrospray pyrolysis method', Materials Research Bulletin, vol. 47, pp. 889-895.

[74] Esteban, G.T. (2014) 'Advanced Thin Layer Deposition of Materials for Li-ion Batteries via Electrospray'. A thesis submitted in partial fulfilment of the Requirements of Technical University of Delft for the Degree of Doctor of Philosophy. Delft: Technical University of Delft.

[75] Walsh, M. (1995) University of Louisville Standard Operating Procedures. http://mitghmr.spd.louisville.edu/lutz/resources/sops/. Prudent practices in laboratory, National Research Council.

[76] Gordon, J.E., The Science of Structures and Materials, Scientific American Library, New York, 1988.Howard, W.E., Better displays with organic films, Sci. Am., Feb. 2004, 76-81.

[77] Esteban, G.T. (2014) 'Advanced Thin Layer Deposition of Materials for Li-ion Batteries via Electrospray'. A thesis submitted in partial fulfilment of the Requirements of Technical University of Delft for the Degree of Doctor of Philosophy. Delft: Technical University of Delft.

[78] Powder X-ray diffraction, available at: http://chemwiki.ucdavis.edu/Analytical_Chemistry/Instrumental_Analysis/Diffraction/Powder_X-ray_Diffraction (accessed 10 August 2015).

[79] Peter, E. and Paul, W. (2010) Atomic Force Microscopy, New York: Oxford University Press Inc.

[80] HA_NC, available at: http://www.ntmdt-tips.com/products/view/ha-nc (accessed 10 August 2015).

[81] Esteban, G.T. (2014) 'Advanced Thin Layer Deposition of Materials for Li-ion Batteries via Electrospray'. A thesis submitted in partial fulfilment of the Requirements of Technical University of Delft for the Degree of Doctor of Philosophy. Delft: Technical University of Delft.

[82] Esteban, G.T. (2014) 'Advanced Thin Layer Deposition of Materials for Li-ion Batteries via

Electrospray'. A thesis submitted in partial fulfilment of the Requirements of Technical University of Delft for the Degree of Doctor of Philosophy. Delft: Technical University of Delft.

[83] Song, M.S., Kim, R.H. and Baek, S.W. (2014) 'Is $Li_4Ti_5O_{12}$ a solid-electrolyte-interphase-free electrode material in Li-ion batteries? Reactivity between the $Li_4Ti_5O_{12}$ electrode and electrolyte', J. Mater. Chem. A, vol. 2, pp. 631-636.

[84] Singh, D., George, A and Kumar, R.V. (2013) 'Nanostructured TiO_2 Anatase Micropatterned Three-Dimensional Electrodes for High-Performance Li-Ion Batteries', American Chemical Society, vol. 117, pp. 19809−19815.

[85] Yu, Y., Shui, J.L. and Chen, C.H. (2005) 'Electrostatic spray deposition of spinel Li4Ti5O12 thin films for rechargeable lithium batteries', Solid State Communications, vol. 135, pp. 485-489.

[86] Jili, L., Youqi, Z and Lin W. (2014) 'Lithium Titanate Epitaxial Coating on Spinel Lithium Manganese Oxide Surface for Improving the Performance of Lithium Storage Capability', American Chemical Society, vol. 6, pp. 18742−18750.

[87] Peter, E. and Paul, W. (2010) Atomic Force Microscopy, New York: Oxford University Press Inc.

[88] The working of the SEM, available at: http://materiaux.ecam.fr/savoirplus/mebanglais/principes.html (accessed 10 August 2015).

[89] Newbury, D., Joy, D and Echlin, P. (1986) Advanced Scanning Electron Microscopy and X-ray Microanalysis, New York: Plenum Press.

[90] Bragg's law, available at: https://en.wikipedia.org/wiki/Bragg%27s_law (accessed 10 August 2015).

Appendix

Introduction of characterization methods mentioned in this thesis

1. Atomic force microscopy (AFM)

Atomic force microscopy(AFM) is a technique that mainly applied to image the surface of both insulating and conducting samples. Different from optical or electron microscope, AFM dose not need to form an image by focusing light or electron beam onto the surface, but measures a 3-D image of the sample surface with a sharp probe. The probe consists of a sharp tip with a curvature around 10nm connected to a cantilever. This cantilever is fixed to a relatively larger chip with different dimensions which vary with the probe series. Before scanning, the probe needs to be fixed into a holder which is then fixed into a head. Then, an appropriate position [(DFL(-2), LF(0)] needs to be adjusted in order to deliver the scanned signal to software system successfully. By doing this adjustment, the Laser beam is focused on the backside of the tip of the cantilever. Meanwhile, the reflected laser beam is just arrived at the favorable position on the photodiode. The topographic information of the sample can be obtained from different scanning modes, including non-contact mode, contact mode and semi-contact mode. In this project, all the AFM topographic images were illustrated in the semi-contact mode.

In the semi-contact mode , the resonance frequency of the cantilever which will be used as the oscillating input signal shall be found at first. Then, the oscillating distance between the sample surface and the probe will be found automatically in soft approach process controlled by the computer. The actual movement of the probe will depend on its interaction with the sample surface. The resulting oscillation in the cantilever deflection is measured and compared to the input oscillation to determine the forces acting on the probe. the probe The quality of the topographic image can be improved by changing the value of set point, feed back gain and scanning rate. A schematic drawing of the semi-contact mode setup is shown below[87].

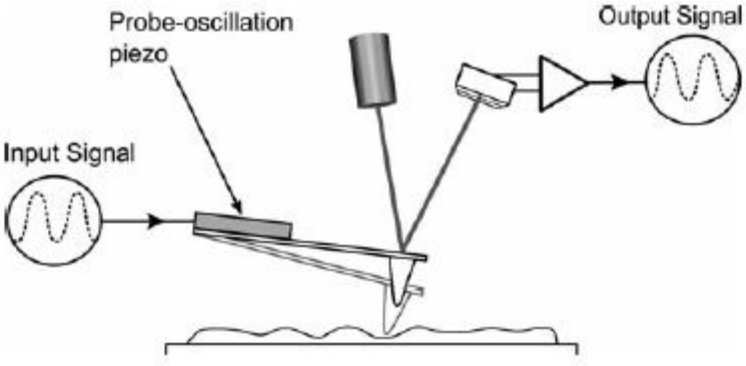

In order to get a good image, the sample used for AFM test should be fixed, keep clean and make sure small enough to be scanned. It should be noted that the quality of the images can also be influenced by the artifacts. For instance, blunt probe, scanner bow, leveling, noises, etc,..

2. Scanning electron microscopy (SEM)

Scanning electron microscopy is a technique that used to produce high resolution images with focused electron beams. A Scanning Electron Microscope usually consists of an electronic optic column built on the sample chamber, a pumping circuit used to obtain a high vacuum, detectors to catch all the signals that the sample gives out, a video screen to examine the pictures and an Electronic device to handle all the functions.

The electron beam will interact with the atoms of the target samples, creating a number of signals, including secondary electrons, back-scattered electrons, characteristic X-rays, auger electrons, etc,.. These signals are emitted at different depth of field and contain different information of the sample, such as surface features and composition, which can be used for characterization. The created electron signals, which are used to modulate the brightness of the screen, can be collected by the detectors and then converted into electric signals an then to be transferred into signal amplificator or energy spectrometer. Deflection coils are used to guide the electron beam to scan at a certain point on the sample surface and, at the same time, link the information to the screen. Then, the quantity of signal produced at a fixed point of the sample is linked to the brightness of the corresponding point on the video screen. A schematic drawing of the structure of SEM is shown below[88].

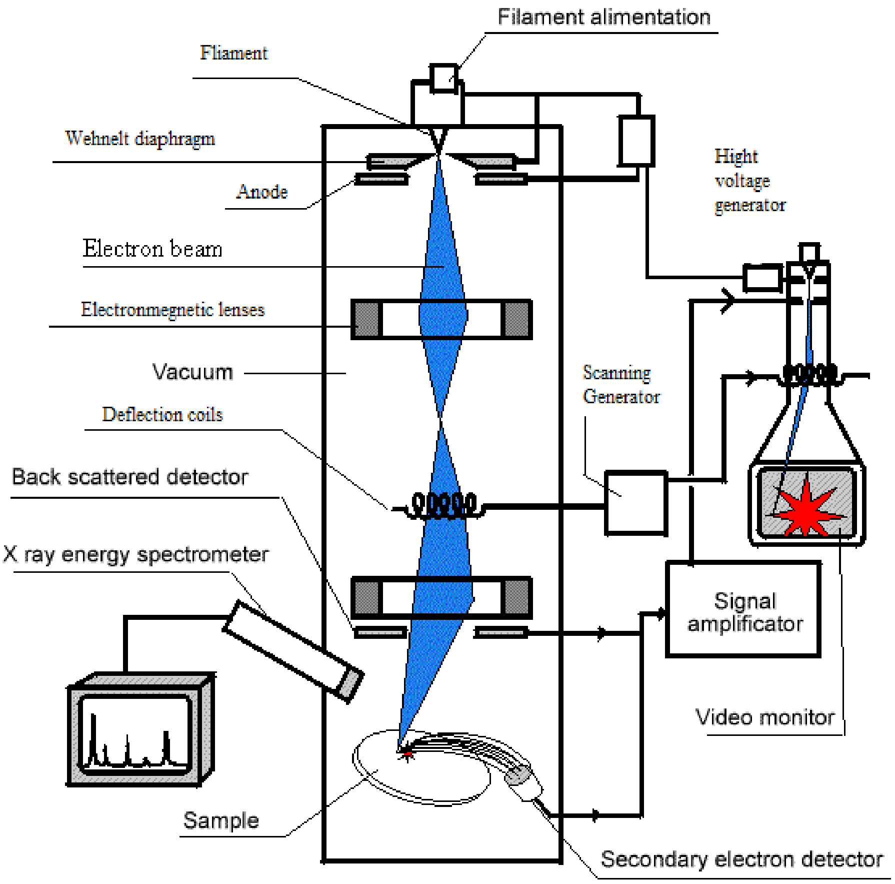

The image results that obtained from this project are secondary electron images (SEI) and back-scattered electron images (BSEI). The secondary electrons are emitted by the inelastic collision between the electron beam and the electrons which move around the atom of the sample. Due to the low energy of secondary electrons (around 50eV), it is easily to be deflected and to be collected by a large amount on the detector, forming a picture with a good signal/noise ratio. They come from the area closed to the beam with only depth and this position gives pictures with good resolution. Therefore, pictures obtained with the detection of secondary electrons mostly represent the topography of the sample.

Back-scattered electrons (BSE) are beam electrons that are reflected from the sample by elastic scattering. The position of BSE detector is set above the sample in the vacuum chamber. BSE are often used in analytical SEM along with the spectra made from the characteristic X-rays, because the intensity of the BSE signal is strongly related to the atomic number (Z) of the specimen. BSE images can provide information about the distribution of different elements in the sample[89].

3. Energy dispersive X-ray spectroscopy (EDS)

Energy dispersive X-ray spectroscopy is applied to identify the type of elements and to investigate the distribution of those elements in the sample. It is usually coupled with back-scattered images in SEM by focusing a high energy electron beam on the specimen. The incident beam may excite an electron in an inner shell bound to a nucleus, ejecting it from the shell while creating an electron hole. An electron from an higher-energy shell then fills the hole at the lower energy orbit by losing energy. This energy may release as the form of X-ray. For different elements, the energy differences between the electron orbits are unique so that the energy of the released X-ray are all different. The number and energy of the X-rays emitted from a specimen can be measured by an energy-dispersive spectrometer and then illustrate a spectrum figure in the software automatically. Comparing the spectrum results with the standard value, the elemental composition of the specimen can be measured. In addition, EDS can also illustrate maps which directly show how the elements distribute in the specimen.

In this project, before EDS measurements start, it needs to increase the electron beam spot size until the cps value falls in the region of 5000-10000 in order to get a more reliable spectrum result. A example figure is shown below.

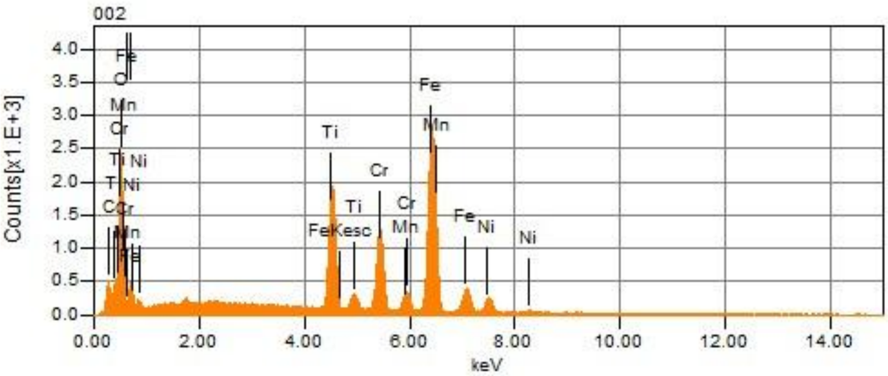

4. X-ray diffraction (XRD)

According to crystal geometry, there are various of crystal structures exist in the nature. For instance, FCC, BCC, spinel, etc,.. Each structure is formed by atoms that occupy the specific positions. Consequently, those atoms can form a series of crystal planes which was signed by miller index, such as (111), (220), (311), etc,.. It should be noticed that different crystal structure can have different planes group. Therefore, crystal structures can be identified by investigating the crystal planes that exist in the specimen.

In this project, X-ray diffraction is used to identify the crystal structure of the sample. The mechanism is based on the theory of elastic scattering of X-ray photons and the Bragg's law. When X-ray photons are incident on a lattice, they will be scattered by the atoms. For the process of elastic scattering, some of these scattered photons will only change their momentum but without losing energy. Those photons can be used to identify the type of the crystal since they carry the information of the distribution of atoms in the lattice structure.

For a crystalline solid, the X-rays are scattered from lattice planes separated by the interplanar distance d. Only when the path length of scattered X-ray is equal to an integer multiple of the wavelength, they can interfere constructively. Otherwise, they will interfere destructively. The path difference between two X-rays undergoing constructive interference is given by $2d\sin\theta$, where θ is the scattering angle (see figure below). The effect of the constructive or destructive interference intensifies because of the cumulative effect of reflection in successive crystallographic planes of the crystalline lattice. The condition for a constructive interference occurs can be simply described as $2d\sin\theta = n\lambda$, which is known as the Bragg's law[90].

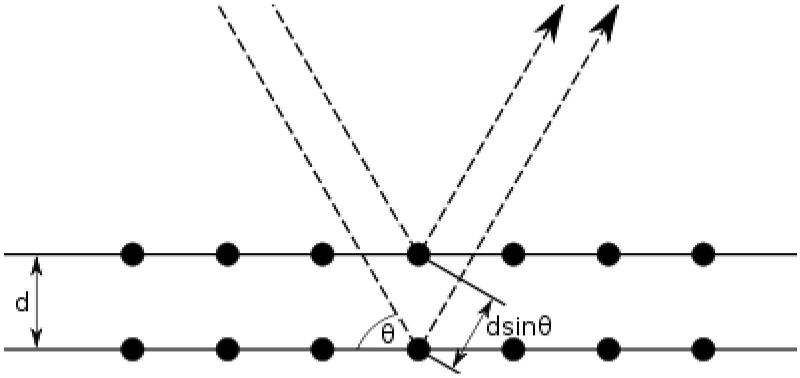

Qiao Pan

4297687

Delft University of technology

Title of the thesis: Effects of $Li_4Ti_5O_{12}$ coating on the performance of $LiNi_{0.5}Mn_{1.5}O_4$ cathode in Li-ion batteries

Supervisors: Dr. Erik Kelder

Raphaël Fredon